SLAC-PUB-11823
astro-ph/0603648

COSMIC EVOLUTION OF BLACK HOLES AND SPHEROIDS. I: THE $M_{BH} - \sigma$ RELATION AT $Z = 0.36$

Jong-Hak Woo[1], Tommaso Treu[1], Matthew A. Malkan[2], Roger D. Blandford[3]

ABSTRACT

We test the evolution of the correlation between black hole mass and bulge velocity dispersion ($M_{BH} - \sigma$), using a carefully selected sample of 14 Seyfert 1 galaxies at $z = 0.36 \pm 0.01$. We measure velocity dispersion from stellar absorption lines around Mgb (5175Å) and Fe (5270Å) using high S/N Keck spectra, and estimate black hole mass from the Hβ line width and the optical luminosity at 5100Å, based on the empirically calibrated photo-ionization method. We find a significant offset from the local relation, in the sense that velocity dispersions were smaller for given black hole masses at $z = 0.36$ than locally. We investigate various sources of systematic uncertainties and find that those cannot account for the observed offset. The measured offset is $\Delta \log M_{BH} = 0.62 \pm 0.10 \pm 0.25$, i.e. $\Delta \log \sigma = 0.15 \pm 0.03 \pm 0.06$, where the error bars include a random component and an upper limit to the systematics. At face value, this result implies a substantial growth of bulges in the last 4 Gyr, assuming that the local $M_{BH} - \sigma$ relation is the universal evolutionary end-point. Along with two samples of active galaxies with consistently determined black hole mass and stellar velocity dispersion taken from the literature, we quantify the observed evolution with the best fit linear relation, $\Delta \log M_{BH} = (1.66 \pm 0.43)z + (0.04 \pm 0.09)$ with respect to the local relationship of Tremaine et al. (2002), and $\Delta \log M_{BH} = (1.55 \pm 0.46)z + (0.01 \pm 0.12)$ with respect to that of Ferrarese (2002). This result is consistent with the growth of black holes predating the final growth of bulges at these mass scales ($\langle\sigma\rangle$=170 km s^{-1}).

Subject headings: black hole physics: accretion — galaxies: active — galaxies: evolution — quasars: general

1. INTRODUCTION

Understanding how and when galaxies form has been a central problem in cosmology for the past few decades (e.g. White & Rees 1978, Blumenthal et al. 1984). One of the main recent developments of this field has been the realization of the key role played by nuclear activity due to accretion onto supermassive black holes (BHs). Nuclear activity and supermassive BHs have been suggested to be relevant for a variety of phenomena, including regulating star formation at galaxy scales via energy feedback to solve the 'downsizing' problem (Cowie et al. 1996; Treu et al. 2005a,b; Bundy et al. 2005; Juneau et al. 2005; De Lucia et al. 2006), providing extra energy to solve the 'cooling flow' problem (e.g. Dalla Vecchia et al. 2004, and references therein), and altering the inner regions of early-type galaxies to solve the 'inner cusp/core' problem (Milosavljevic, et al. 2002; Graham 2004; Boylan-Kolchin, Ma & Quataert 2004).

The best supporting evidences for a strong connection between galaxy formation and nuclear activity are the tight empirical scaling relations connecting the mass of the central supermassive BH with global properties of the host galaxy, such as bulge luminosity (McLure & Dunlop 2002; Marconi & Hunt 2003) and mass (Magorrian et al. 1998, Häring & Rix 2004), galaxy-light concentration (Graham et al. 2001), and stellar velocity dispersion (Gebhardt et al. 2000; Ferrarese & Merritt 2000). The latter correlation, the so-called $M_{BH} - \sigma$ relation has received particular attention for its tightness, which has been suggested to be consistent with no intrinsic scatter (but see Novak, Faber & Dekel 2006 for a statistical analysis of the existing correlations).

The extension of the known empirical correlations between galaxy properties at kpc scales (such as the Fundamental Plane, Dressler et al. 1987; Djorgovski & Davis 1987) to the pc scales of the sphere of influence of the central BH indicates that the formation and evolution of galaxies and supermassive BHs are connected at a fundamental level.

The variety of scales involved makes this a challenging topic to study from both a theoretical and an empirical point of view. From a theoretical point of view, even the most advanced numerical cosmological simulations (e.g. Springel et al. 2005) do not have enough dynamical range to resolve the scales relevant to the central BH. Thus, theoretical studies generally follow one of these two approaches (see, e.g., Stiavelli 1998, Miralda-Escudé & Kollmeier 2005, and references therein for different approaches): i) studying the scaling relations of remnants of mergers of cosmologically inspired progenitors, simulated in as much physical detail as possible (e.g. Robertson et al. 2005); ii) adopting a semi-analytic approach where the effects of nuclear activity are coupled to dark matter merging trees via analytic empirical recipes, similar to the way interstellar medium and stars are treated (e.g. Kauffmann & Haenelt 2000; Volonteri et al. 2003; Menci et al. 2003; Vittorini, Shankar & Cavaliere 2005; Croton et al. 2005; Cattaneo et al. 2005).

The results of these calculations clearly illustrate the complexity of the problem. Even imposing the local scaling relations as the end-point of the coevolutionary models, many diverse results can be obtained. For exam-

[1] Department of Physics, University of California, Santa Barbara, CA 93106-9530; woo@physics.ucsb.edu, tt@physics.ucsb.edu
[2] Department of Physics and Astronomy, University of California at Los Angeles, CA 90095, malkan@astro.ucla.edu
[3] Kavli Institute for Particle Astrophysics and Cosmology, Stanford, CA, rdb@slac.stanford.edu

Submitted to Astrophys.J.

Work supported in part by Department of Energy contract DE-AC02-76SF00515

ple, in terms of numerical simulations of mergers, it appears that the scaling laws can be either preserved or destroyed during a merger, depending on the properties of the progenitors (e.g. dry or gas rich), and the uncertain fate of the central BHs (merger with mass conservation, mass-loss through gravitational radiation, and ejection). When these results are placed into a cosmological framework for the progenitors, a prediction on the evolution of the $M_{BH} - \sigma$ relation can be obtained. For example, Robertson et al. (2005) predict that the relation should evolve in the sense of velocity dispersion increasing with redshift for a fixed BH mass. Analogously, depending on the details of the modeling of gas accretion on the central BH and assembly of the stellar mass, semi-analytic models can predict the evolution of the scaling relations, with a variety of outcomes. For example, Kauffmann & Haehnelt (2000) find the $M_{BH} - \sigma$ relation to be constant with redshift – providing a natural explanation for its tightness– while Croton (2005) finds that stellar mass (and hence presumably velocity dispersion) decreases as a function of redshift for a fixed BH mass.

From the observers' point of view, three main lines of inquiry are being pursued to reconstruct the coevolution of spheroids and BHs. Firstly, improving the determination of the local scaling laws, e.g. extending the samples in size and dynamic ranges, measuring their coefficient, scatter and distribution of residuals. The local relationships are the foundation of the BH-galaxy connection, and contain important evolutionary clues in the form of 'fossil evidence'. For example, Nipoti et al. (2003) find it impossible to preserve all scaling laws during collisionless mergers, and use this finding to rule out dry mergers as the only mechanism for spheroid formation (see also Ciotti & Van Albada 2001; Kazantsidis et al. 2005; Treu et al. 2006). In addition – if selection effects are properly taken into account – the intrinsic scatter of the correlation can be used to constrain formation models (Robertson et al. 2005; Wyithe & Loeb 2005). Increasing the number of objects with well-measured BH mass – through stellar and gas kinematics for inactive BHs or reverberation mapping for active nuclei– is painstakingly difficult with present technology, but nevertheless important progress is being made (see, e.g., Peterson et al. 2005) and substantial improvement is expected with the next generation of telescopes and adaptive optics systems.

The second line of evidence (e.g. Soltan 1982) is provided by the demographics of galaxies and active galactic nuclei (AGNs). Since the energy irradiated by nuclear activity is often supposed to be proportional to the mass accretion rate onto the BH, the luminosity function of AGN and its evolution measure the build up of BHs, although the mass accretion rate could be much higher at high redshift. Among other results – e.g. on the consistency of the mass function of local BHs with that inferred from the accretion history (Salucci et al. 1999; Yu & Tremaine 2002; Marconi et al. 2004; Shankar et al. 2004)– this kind of arguments points towards an anti-hierarchical ('downsizing') growth of BHs, with the more massive BHs ($> 10^8 M_\odot$) growing at earlier times ($z \sim 1-3$) with respect to their less massive counterparts (Marconi et al. 2004; see also Small & Blandford 1992; Tamura, Ohta, & Ueda 2005; Merloni 2004; Heckman et al. 2004). Taking a further step, Merloni, Rudnick & di Matteo (2004) combine the BH mass accretion history with the star formation history of the Universe to find that the growth of BHs appear to predate that of bulges. In other words, the bulge-to-BH mass ratio is a decreasing function of redshift, consistent – at least qualitatively – with independent evidence for significant mass assembly in spheroids since $z \sim 1.5$ (Bell et al. 2005; Treu et al. 2005a,b; Bundy et al. 2005) and for similarities between the star formation histories of active and inactive galaxies (Hunt et al. 1997,1999; Hunt & Malkan 2004; Woo et al. 2004, 2005). In this scenario, BHs would reach their almost final mass early-on and then the bulge would grow around them, with the local scaling-laws as the evolutionary end-point.

The third approach consists of measuring directly the evolution of scaling laws over cosmic time. The main obstacle to overcome to reach this goal is the determination of the BH mass at distances where the sphere of influence (with a radius $\sim GM_{BH}\ \sigma^{-2}$) cannot be resolved. This approach is thus limited to active BHs, where the mass of the BHs can be inferred from the kinematics of the broad emission line region and its distance from the nucleus (obtained via reverberation mapping or some empirically calibrated surrogate, see § 4). In turn, by restricting the analysis to active BHs, it is more difficult to measure the properties of the host galaxy, and it is important to understand any caveats introduced when comparing to the local benchmark sample of mainly non-active galaxies.

In spite of the challenges and the limitations, this approach is the only one that allows a direct mapping of the coevolution of BHs and spheroids, and thus is an extremely valuable complement to the first two described above, lifting many of the degeneracies introduced by evolution (fossil evidence) or by population averages (BH and galaxy demographics). For these reasons a few groups have been attacking the problem using different observational strategies. Walter et al. (2004) use spatially resolved radio observations to estimate the mass of the host galaxy of a QSO at z=6.41, with a result almost two orders of magnitude smaller than predicted by the local BH-spheroid relation for the value of BH mass measured by Willott et al. (2003). In contrast, Shields et al. (2003) use the width of the [O III] narrow line as a surrogate for the stellar velocity dispersion of a sample of bright QSO, finding no evidence for evolution of the $M_{BH} - \sigma$ relation out to $z \sim 3$, although with a large scatter.

Our group is following a different approach, taking smaller steps in redshifts and striving to achieve the most accurate possible measurements of each parameter. As described in our first paper (Treu, Malkan & Blandford 2004, hereafter TMB04), we target Seyfert 1 galaxies to simultaneously measure AGN broad line width and host galaxy stellar velocity dispersion in specific redshift intervals, where sky emission and absorption can be avoided (see § 2.1). Our pilot study found tentative evidence of evolution, in the sense that our 7 objects had smaller velocity dispersion for given BH mass than expected from the local correlations.

This paper seeks to expand and improve on the pilot study in order to verify this tantalizing and perhaps surprising finding. The main improvements over the previous study include: i) a larger dataset (20 objects) with

better quality Keck data (S/N up to 100Å^{-1} as opposed to $\sim$ 50 Å^{-1} of the pilot study and thus smaller uncertainty on the velocity dispersion; ii) higher completeness to limit possible selection effect (14/20 velocity dispersions measured as opposed to 7/13); iii) a detailed analysis of many potential sources of systematic uncertainties, including that due to the broad nuclear Fe II contamination to the spectral region used for velocity dispersion measurement; iv) improved estimates of BH masses based on the extensive work done by Peterson et al. (2004) and Onken et al. (2004) to calibrate the scaling relations between continuum luminosity, Hβ width and BH mass. High resolution images taken with the Advanced Camera for Surveys (ACS) on board the Hubble Space Telescope (HST) are also available and will be used in this paper to interpret the results (a detailed analysis of the HST-ACS images will be presented in the second paper of this series, hereafter Paper II).

The paper is organized as follows, In § 2 we describe sample selection, observations and data reduction. In § 3 we describe stellar velocity dispersion measurements and discuss the viability of [O III] as a surrogate for stellar velocity dispersion. In § 4 we derive the BH mass and discuss its relation with other AGN properties. In § 5 we present the evolution of the $M_{BH} - \sigma$ relation. Section 6 summarizes a number of tests aimed at investigating possible systematic uncertainties. In § 7 we discuss our results and their implications for the coevolution of spheroids and BHs. Section 8 concludes with a brief summary. Throughout the paper we adopt a cosmology with $\Omega = 0.3$, $\Lambda = 0.7$, and $H_0 = 70$ km sec^{-1} Mpc^{-1}.

2. OBSERVATIONS AND DATA REDUCTION

2.1. *Sample Selection*

As in our pilot study, the choice of targets is key to the success of this experiment. On the one hand, the sphere of influence of supermassive BHs in galaxies at cosmological distances cannot be resolved even with HST. Therefore, it is necessary to target active galaxies, where BH mass can be obtained from the integrated properties of the broad line region – as described in Section 4. On the other hand, in order to measure the *stellar velocity dispersion* from absorption lines, we need to target relatively low luminosity AGNs where the fraction of stellar light in the integrated spectrum is non-negligible. This is because in distant galaxies, ground-based telescopes cannot separate the emission of the host galaxy from that of the AGN.

Seyfert 1 galaxies provide the right balance between the two components: absorption features typical of old stellar populations such as the Mgb triplet ($\sim$ 5175Å) and Fe (5270Å) (Trager et al. 1998) are clearly visible in their high S/N integrated spectra. In order to minimize the systematic uncertainties related to sky subtraction and atmospheric absorption corrections, it is convenient to select specific redshift windows where the relevant emission and absorption lines (Hβ, Mgb, and Fe) fall in clean regions of the Earth's atmosphere. Accordingly, we selected the "clean window" $z = 0.36 \pm 0.01$, which corresponds to a look-back time of ~ 4 Gyrs.

A first object (MS1558+453; hereafter S99; Stocke et al. 1991) was selected for a pilot study (see TMB04). When the Sloan Digitized Sky Survey (SDSS) became available, a larger sample of objects was selected according to the following criteria: $0.35 < z < 0.37$, and Hβ equivalent width and gaussian width greater than 5 Å in the rest frame. All SDSS spectra satisfying these criteria were visually inspected by two of us (TT and MAM) and objects showing strong Fe II nuclear emission (the main obstacle to velocity dispersion measurement) were eliminated from the sample.

The relevant properties of the observed objects are listed in Table 2. Although targets were initially selected from the SDSS DR1 and DR2, all SDSS related quantities listed in this paper have been updated to reflect all the recalibrations available from DR4. Throughout this paper we will make limited use of morphological information derived from an ongoing imaging program with the Advanced Camera for Surveys on board HST (GO-10216; PI Treu) to interpret our results.

2.2. *Observations*

High S/N ratio spectra of 20 targets were obtained with the LRIS spectrograph at the Keck-I telescope in five runs between March 2003 and July 2005. The 900 lines mm^{-1} grating centered at 6700Å was used most of the time, yielding a pixel scale of 0.85Å×0.″215 and a resolution of $\sim$55 km s^{-1}. For two objects, S28 and S29, we used the 831 lines mm^{-1} grating, with which $\sim$67 km s^{-1} resolution was obtained. Observing conditions were generally mediocre, plagued by cirrus and humidity, except for the last runs in May 22 2004 and July 2005. Table 1 shows the journal of observations and instrumental setups. Typically more than two exposures per object were obtained to ensure proper cosmic ray removal, with total exposure times ranging between 600 and 12600 seconds. Taking advantage of the good observing conditions, the exposure times for the last observing run were much higher than in previous runs and some objects with marginal quality spectra were reobserved with longer exposure times (e.g. S05 was observed for 3 hours in addition to the 0.5 hrs obtained during the September 2003 run).

Internal flat fields were obtained before and after observing each object, so as to correct the fringing pattern of the red CCD. A set of A0V stars, selected from the Hipparcos catalog[4] to be within $\lesssim$ 15 degrees from each target, was observed during the night as secondary flux calibrators and to measure the B-band atmospheric absorption. Spectrophotometric standards were observed at the beginning and at the end of each night.

2.3. *Data Reduction*

The standard data reduction processes including bias subtraction, flat-fielding, spectral extraction, wavelength calibration, and flux calibration were performed using a series of IRAF scripts. Cosmic rays were removed from each individual exposure using the Laplacian cosmic ray identification software (van Dokkum 2001). Sky emission lines were used for wavelength calibration.

Optimal extraction was used for obtaining one-dimensional spectra with maximal S/N. Typical extraction radius was 4–5 pixels, corresponding to $\sim 1''$ ($\sim$ 5 kpc at $z = 0.36$). Individual spectra were combined with inverse-variance weighting to make the final spectrum

[4] URL http://www.gemini.edu/sciops/instruments/niri/NIRISpecStdSearch.h

(S/N is in the range of 31 to 111 per 0.85Å pixel for the combined spectra). The relatively featureless spectra of the A0V Hipparcus stars were used to correct the atmospheric absorption (including the prominent B-band) and perform relative flux calibration. Internal tests show that this procedure yields the necessary correction of the B-band absorption to a level of a few parts in a thousand and relative flux calibration to a few percent (confirmed also by comparing our spectra to the SDSS spectra).

The final flux-calibrated spectra of all 20 observed AGNs are shown in Fig. 1. Note the higher S/N ratio of spectra obtained in 2005 with respect to the older spectra.

3. STELLAR VELOCITY DISPERSION MEASUREMENTS

Stellar velocity dispersions of external galaxies are often measured from strong absorption lines such as the G-band (4304Å), the Mgb triplet ($\sim$ 5175Å), Fe (5270Å), and the Ca II triplet ($\sim$ 8550 Å). For the host galaxies of broad line AGNs, the G-band is impractical due to contamination from Hγ, while the Mgb-Fe and the Ca II triplet regions represent viable choices, provided spectra of sufficiently high S/N are available (Nelson & Whittle 1996; Barth et al. 2003; Woo et al. 2004; Greene & Ho 2005c). In this study, we focus on the Mgb-Fe region, since the Ca II triplet is redshifted outside the wavelength range accessible with optical spectrographs.

Higher S/N than for quiescent galaxies is needed to compensate for the dilution of stellar features by the AGN continuum, scaling as $1/f_*$ where f_* is the fraction of stellar light in the integrated spectrum. Systematic errors such as those due to correction for atmospheric absorption must also be smaller than for quiescent galaxies by a factor of f_* to account for line dilution. As discussed in Section 3.2, the quality of our spectra is sufficient to recover velocity dispersion with an uncertainty of 10% or better.

However, before we can proceed to measure velocity dispersion, we need to address an important possible source of systematics, contamination of the AGN power-law continuum by broad nuclear Fe II emission. In our pilot paper the Fe II contribution was removed using high order polynomials. In this paper we improve on our Fe II emission subtraction by using the I Zwicky 1 local Fe II template (Boroson & Green 1992; kindly provided by Todd Boroson) as described in the next Section.

3.1. *Fe II Subtraction*

In the case of host galaxies of type 1 AGNs, strong Fe II emission around 5150-5350Å complicates velocity dispersion measurements from the Mgb and Fe lines since the observed continuum shape is very different from that of template stars. To reduce potential systematic errors on dispersion measurements, we decided to subtract broad Fe II emission from the observed spectra before fitting with template stars (for a consistency check, we also measured velocity dispersion from spectra without Fe II emission subtraction. See § 6.1.2).

We subtracted broad Fe II emission using the I Zw 1 template. First, following Boroson & Green (1992), we prepared a set of Fe II templates with various widths and strengths. Then, for the purpose of this fit, we added a power-law spectrum representing locally the featureless AGN continuum, and a constant representing the stellar component[5]:

$$F(\lambda) = a \times \lambda^{\alpha} + b \times FeII(\lambda, v) + g, \qquad (1)$$

where α is the continuum slope, v and b set width and strength of Fe II template, and g represents the stellar flux. For each set of parameters, the model spectrum was compared with observed spectra to compute the χ^2. By χ^2 fitting, we derived the best fit width and strength of broad Fe II emission, and the slope of AGN continuum as demonstrated in Fig. 2. Since we are interested in removing broad Fe II emission to ease the stellar velocity dispersion measurements, we only used the 5100-5400Å region to fit the Fe II emission.

The Fe II emission subtracted spectra are compared with the observed spectra in Fig. 3. We note that there is a range of Fe II emission strengths (3–24% in total luminosity at 5100-5500Å). Fe II emission is stronger for S01, S03, S05, S07, S10, S11, S21, S29 while Fe II emission is negligible for other cases. Stellar absorption features are clearly shown in many AGN spectra. However, we can not identify stellar lines for 6 objects, i.e. S02, S03, S10, S21, S27, and S29, most likely due to the much higher AGN continuum.

3.2. *Stellar Velocity Dispersion Measurements*

Velocity dispersions were obtained by comparing in pixel space the observed host galaxy spectra with stellar templates broadened with a Gaussian velocity width ranging between 50-400 km s^{-1}. We used as kinematic templates high resolution spectra of 5 giant stars (spectral types: G8, G9, K0, K2, and K5) observed with ESI on Keck-II (Sand et al. 2004). Fits were performed for every template to estimate uncertainties due to template mismatch, while the best fitting template was used for the final dispersion measurements.

The minimum χ^2 fit was performed using the Gauss-Hermite Pixel Fitting software[6] (van der Marel 1994). The merit of fitting in pixel space as opposed to Fourier space is that typical AGN narrow emission lines (e.g. [Fe VII] 5160Å, [N I] 5201Å, and [Fe XIV] 5304Å; Vanden Berk et al. 2001) can be easily masked out (e.g. Barth et al. 2002; TMB04; Woo et al. 2004; see Fig. 4). Extensive tests, fitting in various spectral regions including Mgb 5175Å and Fe 5270Å, were performed to determine the best spectral regions. As expected, we find that the Fe line at 5270Å is most useful in the cases when the Mgb triplet is mostly affected by narrow AGN emission lines (see Greene & Ho 2005c). Low order polynomials (2-3) were used to model the overall shape of the continuum. For 14 out of 20 objects we determined reliable velocity dispersions, i.e. robust with respect to changes of template, continuum polynomial order, and fitting region. The final measurements are listed in Table 3. For the subsample in common with TMB04 the values listed in Table 3 supersede those in the pilot study, given the improved data quality and analysis.

3.3. *[O III] line width vs. stellar velocity dispersion*

[5] Since the stellar features are much narrower and often shallower than the nuclear Fe II emission, this is an appropriate approximation for this purpose

[6] Available at http://www.stsci.edu∼marel/software.html

Narrow-line clouds have been suggested to be bound predominantly by the gravitational potential of the host galaxy bulge (Nelson & Whittle 1996), providing an opportunity to use the width of [O III]λ5007 as a readily measurable surrogate for stellar velocity dispersions. This method has been applied to higher redshifts and less favorable AGN-to-stellar light ratios (e.g. Shields et al. 2003).

The characteristically asymmetric profile of the [O III] lines (e.g. Fig. 1) implies that this assumption is an approximation and some non-gravitational broadening is present (see Boroson 2005). In fact, several studies show that the [O III] width can trace the velocity dispersion only in a statistical sense when a large sample is available (Boroson 2003; Nelson et al. 2004; Bonning et al. 2005; Greene & Ho 2005a; Hicks 2005), and when appropriate care is taken in dealing with the wings of the line profile.

Here we take advantage of our high quality spectra to revisit the question of what the best proxy is, i.e. what measure of the [O III] line width provides the tightest and least biased correlation with stellar velocity dispersion.

We measured [O III] line widths in three different ways, commonly used in the literature. First, we fitted [O III] with a single gaussian, as typically done with low S/N spectra. Second, we measured the FWHM from its definition (e.g. Brotherton 1996; Bonning et al. 2005). Third, we removed the blue wing – present for all 14 objects – by fitting two Gaussian components (e.g. Greene & Ho 2005a). All these measurements were done with the SPLOT task in IRAF after subtracting the continuum.

In Fig 5, we compare the stellar velocity dispersion with [O III] velocities obtained with three different methods, assuming $\sigma_{OIII} = FWHM/2.35$ when necessary. As expected, since all 14 objects show clear asymmetry with a blue wing, a single gaussian component does not provide a good fit and the proxy generally overestimates the stellar velocity dispersion by 15% on average (left panel), i.e. $\Delta \log \sigma = 0.065$. The simple FWHM does a better job, reproducing the stellar velocity dispersion with an average offset of less than 5% (center panel). In contrast, when the blue wing is removed, [O III] line widths are systematically smaller leading to an underestimate of the stellar velocity dispersion by almost 20%. We find similar scatter for all cases $\sim 25\%$, smaller than 0.2 dex found by Nelson & Whittle (1996; see also Onken et al. 2005), but still a significantly larger uncertainty than what can be achieved via direct determination (10%) from stellar absorption features.

Although based on this test the FWHM appears to be the best [O III] based proxy for the stellar velocity dispersion, the non-gravitational broadening may depend on properties such as accretion rate (e.g. Greene & Ho 2005a) and therefore our results may not apply to *all* kinds of AGNs. What appears to be a solid conclusions is that the intrinsic scatter is larger than typical error on the stellar velocity dispersion. The results from this section will be used in § 7 when discussing our results in comparison with other studies based on the [O III] proxy.

4. BLACK HOLE MASS ESTIMATION

The mass of supermassive BHs beyond the local universe cannot be directly measured from the spatially resolved kinematics because of the limited spatial resolution of the current instruments. In the case of AGNs, the size of the broad-line region, R_{BLR}, can be measured via reverberation mapping (Blandford & McKee 1982). Combining the size of the broad line region with its kinematics, as inferred from the line width, gives the mass of the BH up to a 'shape' factor of order unity which depends on the three-dimensional geometry and kinematic structure (Peterson 1993; Peterson et al. 2004). The shape factor has recently been calibrated by Onken et al. (2004), by requiring active galaxies to obey the same $M_{BH} - \sigma$ relation as quiescent galaxies.

However, reverberation mapping requires long-term monitoring and it is extremely expensive to obtain for a large sample of AGNs, especially at high-redshift. Instead, the so-called 'virial' BH mass is often estimated from a single-epoch spectrum using the empirical radius-luminosity relation, i.e. the correlation between R_{BLR} and the optical luminosity at 5100Å (Kaspi et al. 2000; Kaspi et al. 2005). On physical grounds, R_{BLR} is expected to scale as the square root of the luminosity in ionizing photons. Although the exact dependence on the optical luminosity cannot be calculated directly from first principles, it has been calibrated empirically (Wandel, Peterson & Malkan 1999; Kaspi et al. 2005). For this reason we will refer to the method used to obtain BH masses in this paper as empirically-calibrated photoionization (ECPI) method.

In this paper we adopt the latest calibrations (Onken et al. 2004; Kaspi et al. 2005) of the local reverberation mass shape factor of the R_{BLR}-L_{5100} relationship, to derive BH masses:

$$M_{\rm BH} = 2.15{\times}10^8 {\rm M}_\odot {\times} \left(\frac{\sigma_{H\beta}}{3000 {\rm kms}^{-1}}\right)^2 \left(\frac{\lambda L_{5100}}{10^{44} {\rm ergs}^{-1}}\right)^{0.69}, \quad (2)$$

where $\sigma_{H\beta}$ is the second moment of the Hβ line profile and L_{5100} is the monochromatic luminosity at 5100Å, in the rest frame, measured as discussed in the next sections. Based on comparisons of reverberation data and single-epoch data (Vestergaard 2002; see also § 6.2.1), it is estimated that the intrinsic uncertainty associated with this method is approximately a factor of 2.5, i.e. 0.4 dex, on the BH mass. This uncertainty dominates the errors on our input quantities, $\sigma_{H\beta}$ and L_{5100}, and we adopt it as our total uncertainty on the BH mass.

In closing, we note that the normalization of Onken et al. (2004) – confirmed by Greene & Ho (2005b) on single-epoch data – increases BH mass by 0.26 dex compared to the previous standard shape factor, (arbitrarily) calculated assuming of isotropic distribution of broad-line clouds. We emphasize, however, that when measuring the *evolution* of the $M_{BH} - \sigma$ relation, we will use the *same* shape factor for the local and distant sample, so that the specific choice of the shape factor is irrelevant as long as it is constant with redshift.

4.1. *Hβ width measurements*

The width of Hβ is measured in five steps as in our previous work (TMB04; the procedure is illustrated in Fig. 6 for all the objects in the sample). First, we identify the continuum level on each side of Hβ. We typically used 50Å windows in the range 4690-4780Å and 5010-5130Å to measure the the blue and red continuum levels. We then subtracted the continuum by linear interpolation. Second, we subtracted [O III] λ4959 by dividing

[O III] λ5007 by 3 and blueshifting. Third, we rescaled [O III] λ5007 and blueshifted it to subtract the narrow component of Hβ. The flux ratio of Hβ/[O III] λ5007 is found to be in the range 6-16%, consistent with other studies (e.g. Marziani et al. 2003). Fourth, we measure the second moment of the line profile for minimum (zero) and maximum acceptable narrow components. When the Hβ profile is very large and clearly goes under [O III] λ5007 line, we obtained this red wing shape by reflecting the blue wing around the centroid of the broad component.

The statistical noise on the measurement is negligible, given the quality of the spectra. The three potential sources of systematic error are removal of the narrow core of Hβ, the definition of the continuum level, and the contribution to the second moment of broad Hβ from the wavelength region under [O III] λ5007. Varying the intensity of the narrow component of Hβ changes the second moment by only a few per cent, which is negligible for our purposes. Changing the wavelength regions defining the continuum level does not significantly affect the line width except for the case of S99, where there is a distinct core superposed on a much broader redshifted component. The low contrast and large width of the latter component makes its measurement particularly sensitive to the choice of continuum. Similar profiles are sometimes observed in the low states of local Seyfert 1 galaxies such as NGC 3227 and NGC 3516 (Rosenblatt et al. 1994). If the red continuum were chosen to be at the base between the [OIII] 4959 and 5007 lines, the second moment would be reduced by a factor of 2, resulting in a smaller BH mass estimate by a factor of 4. However, as in those local galaxies, it is clear that the Hβ wing actually does extend to larger positive velocities than 8000 km sec^{-1}, so that the continuum we chose on the red side of 5007 is more realistic. The conclusions of this paper are unchanged if the narrower line width is adopted for S99.

Three objects, namely, S12, S21 and S23 show a prominently asymmetric broad-line profile. The extension of the line underneath [O III] λ5007 is therefore unclear, and could result in a small uncertainty. We measured for these objects line widths with/without Hβ wing underneath of [O III] λ5007, and find less than 4% change, suggesting that errors due to red wing of Hβ are negligible. A final potential source of uncertainty is contamination from broad Fe II features in the region between 4861 and 5007 Å rest frame. For consistency with the analysis performed on local calibrators (Kaspi et al. 2005), we do not attempt to remove this component. In section 6.2.1 we show that this source of uncertainty is negligible, by comparing our measurement of Hβ from single-epoch spectra with that obtained from the rms spectra of Peterson et al. (2004).

4.2. *Luminosity at 5100 Å*

We directly measured the optical luminosity around 5100Å from the observed spectra defined as the average flux in the 5070-5130Å region in the rest frame. Considering the difficulty of achieving absolute flux calibration for the Keck spectra – due to slit losses, variable seeing and sky transparency– we tied our spectrophotometry to the extinction corrected r' band magnitude taken from the SDSS-DR4 archive. First, we measured the r' band magnitude from our observed spectrum using the corresponding response function. Then, we calculated the offset between Sloan and our measured magnitude, to correct the measured flux. The mean offset is 0.44 ± 0.10. We did not correct for the stellar contribution to the luminosity at 5100Å, to be consistent with reverberation calibrators. We will discuss the effect of stellar contamination in § 6.2.2.

5. THE $M_{BH}-\sigma$ RELATION AT $Z = 0.36$

Having measured velocity dispersions and BH masses, in this section we derive the $M_{BH}-\sigma$ relation of our sample of Seyferts at $z = 0.36$, and compare it with the local samples to infer evolutionary trends.

Fig. 7 shows our $M_{BH}-\sigma$ in comparison with the local relationship for quiescent galaxies as measured by Tremaine et al. (2002; solid line; hereafter T02) and by Ferrarese (2002; dashed line; hereafter F02). Given the small average difference of velocity dispersion ($\lesssim$3–4% for the sample in common) between T02 and F02, we neglect aperture effects (see also discussion in Merritt & Ferrarese 2001 and in T02). An upper limit to the systematic uncertainty due to the different apertures adopted in our sample and those adopted for the local samples is given in § 6.1.3.

Two things are immediately apparent: 1) all points are above the local relationship, that is smaller velocity dispersion for a fixed BH mass; 2) apart from an overall offset and the relatively narrow range in BH mass, the relationship appears relatively tight even at this redshift, as we will quantify later in this section. The small scatter (0.35 dex in BH mass) – reduced with respect to our previous measurement (TMB04) – is encouraging and consistent with a decrease of the uncertainties due to the improved data quality and analysis.

5.1. *Redshift evolution*

In order to improve the measurement of the offset from the local relationship and the amount of scatter, and to assure that we are comparing the same kind of objects, we introduce in Fig. 8 two additional comparison samples, composed of active galaxies at lower redshift: the 14 reverberation mapped AGNs with mean redshift of 0.02 from Onken et al. (2004), and the 15 dwarf Seyfert galaxies with mean redshift of 0.08 from Barth et al. (2005). BH masses of our sample and Barth et al. are consistently estimated using Eq. 2, which is calibrated on the reverberation masses available for the Onken et al. sample (see Greene & Ho 2005b for an additional check on the local calibration of the ECPI method masses). In other words, a change in the shape factor will move the three samples vertically by the same amount.

By design, the Onken et al. points straddle the local relationships. The Barth et al. points tend to lie preferentially above the local relationships with an average offset, of which the exact amount depends on the local slope. The $z = 0.36$ points are definitely above the local relationship. This is illustrated in Fig. 9, where we show the offset from the local relationship of T02 as a function of redshift for all the points in the individual samples. The average and rms scatter of each sample is shown as solid red symbols with error bars.

The offset is clearly detected and appears to increase with redshift. The best linear fit to the data is shown

as a solid line (for the three samples) and a dashed line (excluding the sample of dwarf Seyferts from Barth et al. 2005). The best fit linear relationship for all three samples is $\Delta \log M_{BH} = (1.66 \pm 0.43)z + (0.04 \pm 0.09)$. The rms scatter of the $z = 0.36$ sample is 0.35 dex, similar to that of the Onken et al. sample and to the estimated uncertainty of the BH masses via ECPI. The average offset of the $z = 0.36$ sample is 0.62 ± 0.10 dex in BH mass, corresponding to 0.15 ± 0.03 in $\Delta \log \sigma$. A somewhat larger scatter is found for the Barth et al. sample (0.5 dex), but still remarkably small, considering that their measurement relies on an extrapolation of the radius-luminosity relation outside the parameter space of the reverberation mapped calibrators.

Adopting the local relationship of F02 does not significantly change the offset of the Onken et al. points and marginally changes the offset of our points (0.57 ± 0.11 dex) while it does increase the offset of the Barth et al. points from 0.32 ± 0.15 to 0.45 ± 0.15 dex. This is due to the difference of the local M_{BH}-σ relationships for BH masses of order $10^6 M_\odot$. Including only our points and the Onken et al. points, the best fit offset with respect to the F02 relation is $\Delta \log M_{BH} = (1.25 \pm 0.49)z + 0.17 \pm 0.10$. Even in this case, we detect evolution in the form of a non-zero slope. For all three samples, the linear relationship is $\Delta \log M_{BH} = (1.55 \pm 0.46)z + 0.01 \pm 0.12$.

A final important point concerns the morphological type of the host galaxies. The local samples of T02 and F02 are composed of mainly elliptical and S0 galaxies, while our sample comprises mostly spiral galaxies (see Table 3). Thus, if – as discussed in Section 7– the $M_{BH} - \sigma$ relation depends on morphological type, comparing our sample to the local quiescent sample could introduce a selection bias. However, since the comparison sample of Onken et al. is quite similar to ours in terms of distribution of host galaxy morphological types, this does not appear to be a problem. Within the limited size of our sample, we can explore a possible dependency of the $M_{BH} - \sigma$ relation on morphological type by considering the offset for two distinct subgroups, the bulge-dominated (i.e. ellipticals, lenticulars, and Sa; red solid squares in Fig. 7) and the disk-dominated (Sb, Sc; solid blue triangles). For the 4 bulge-dominated systems we find an average offset of 0.42 ± 0.16 dex in BH mass, indicating that the offset of bulge-dominated systems is still significant. In the case of 9 disk-dominated systems we find an offset of 0.75 ± 0.10 dex. Within the small number statistics of the subsamples, this suggests that bulge-dominated systems are closer to the local $M_{BH} - \sigma$ relation, consistent with a scenario that the local relation is the end-point of galaxy evolution as we will discuss in § 7.

6. TESTING SYSTEMATIC UNCERTAINTIES

Before discussing the interpretation of our results in Section 7, we need to understand systematic errors. In this section we list a number of potential sources of error and estimate as accurately as possible the associated uncertainties. We pay particular attention to those effects that could simulate artificially our observed evolution, i.e. those that could lead us to overestimate BH mass or to underestimate the velocity dispersion. To estimate the relevance of the uncertainties, it is useful to keep in mind that the observed offset is 0.62±0.10 in $\Delta \log M_{BH}$ or equivalently 0.15±0.03 in $\Delta \log \sigma$.

6.1. *Are velocity dispersions underestimated?*

6.1.1. *Template mismatch*

Stellar velocity dispersions of early-type galaxies are typically measured by comparison with broadened spectra of Galactic giant stars, which are believed to dominate their integrated light. However, individual stars cannot reproduce perfectly the integrated stellar populations, and template mismatch has long been known as a potential source of error (e.g. Rix & White 1992). To estimate this effect we use a set of templates covering a range of stellar types and find that velocity dispersion is stable, varying by less than the estimated error from one template to another.

Another potential source of error is the mismatch in abundance ratio between galactic templates and those in external galaxies. For example, Barth et al. (2003) and Woo et al. (2004, 2005) found that the Mgb triplet is much stronger in host galaxies of BL Lac objects – which are generally massive galaxies ($> 10^{11} M_\odot$) – due to the α element enhancements, and that trying to fit simultaneously Mgb and Fe could introduce systematic uncertainties (see also Greene & Ho 2005c). Only one of our spectra, S24, shows significant Mgb mismatch, consistent with the overall similarity between the host galaxies and the Milky Way in terms of morphology (see Table 3). In the case of S24, we excluded the Mgb region from the fit (see Fig. 4). For robust measurements, we tested potential systematics due to subtle mismatches on the other spectra by repeating the fits without Mgb and found no significant changes.

We conclude that template mismatch does not introduce significant systematic errors.

6.1.2. *Continuum fit*

The presence of an active nucleus manifests itself in the observed spectra as two main features: 1) a featureless continuum, which dilutes stellar absorption lines; 2) various broad and narrow emission lines. For our sample and in our wavelength range, the AGN features that are relevant to the stellar velocity dispersion measurement are broad Fe II emission at 5100-5400 Å and narrow emission lines in the vicinity of the Mgb triplet. The narrow lines can be dealt with by masking out during the kinematic fit. The robustness of velocity dispersion with respect to masking out the whole Mgb triplet region shows that the narrow lines do not introduce a substantial source of error.

To check the effect of subtracting Fe II, we repeated the measurement of velocity dispersion, using spectra without Fe II subtraction. In this case, we normalized the spectra with a high (5-7) order polynomial fit, before comparing with broadened template stars. The two measurements are compared in Fig. 10. We find the largest difference ($\sim 20\%$) for S07, which has the strongest Fe II emission. Overall, the agreement is quite good, the two different measurements agree with a mean offset of 0.01 dex and a rms scatter of 0.04 dex, much smaller than the offset 0.15 dex in $\log \sigma$. The agreement between the two results suggests that the stellar velocity dispersions are not underestimated due to systematic effects related to the Fe II subtraction.

6.1.3. *Aperture correction*

Our adopted extraction window ($\sim 1'' \times 2'' = \sim 5 \times 10$ kpc^2) is of order of the expected effective radius (r_e) of the bulges in our sample. For comparison, the average and median of the r_e for the sample of early-type galaxies and early-spirals analyzed by Treu et al. (2005) – with velocity dispersion in the same range as our sample – are 3.8 and 2.7 kpc, respectively. We adopt these numbers as our fiducial estimate of the r_e to quantify whether the larger aperture with respect to those in the local studies could introduce a systematic bias in our measured velocity dispersions.

For the local sample of quiescent galaxies, Gebhardt et al. (2000, also Tremaine et al. 2002) used an aperture close to r_e, while Ferrarese & Merritt (2000, also Ferrarese 2002) corrected velocity dispersions to a smaller aperture, 1/8 of r_e. However, the average difference in luminosity-weighted velocity dispersions of the same sample between Tremaine et al. (2002) and Ferrarese (2002) is only a few per cent since most of the light comes from the central part of the bulges (Merritt & Ferrarese 2001; Tremaine et al. 2002). Similarly, when comparing our sample with the local samples, we expect small aperture effects on our luminosity-weighted velocity dispersions. We note that our kinematics is measured from optimally extracted spectra with inverse variance weighting and thus more weighted towards the center than a simple luminosity weighted average.

A conservative upper limit to uncertainty due to the aperture effects can be derived as follows. For early-type galaxies, the standard correction proposed by Jørgensen, Franx & Kjærgaard (1995) implies insignificant correction factors of 1.0% and 2.5% (for the two estimates of r_e) from our aperture to the velocity dispersions measured within r_e as in the Gebhardt et al. (2000) local sample. The correction for the smaller aperture adopted by Ferrarese (2002) is 9.9% and 11.1%. However, the effect is probably smaller when considering seeing effects, luminosity and optimal extraction. For example, Padmanabhan et al. (2004) constructed velocity dispersion profiles based on SDSS fibers corresponding to different fractions of an effective radius, and found them to be flat. As for spirals, recent measurements of the aperture correction factor indicate that the effect is indeed negligible (Pizzella et al. 2004). We conclude that aperture effects ($\sim$ 10% at most, i.e. 0.04 dex in σ) are significantly smaller than what would be needed (0.15 dex in σ) to bring our points at $z = 0.36$ in agreement with the local $M_{BH} - \sigma$ relation.

6.1.4. *Host galaxy morphology and inclination*

The final source of potential systematic error for velocity dispersion that we consider is contamination by kinematically "cold" (i.e. with velocity dispersion smaller than that typical of the bulge) stars in the disk. Mgb and Fe lines arise from relatively old stellar populations (e.g. Trager et al. 2000). Therefore, the contribution from the younger stars in the disks to these lines should be small with respect to the contribution to the optical continuum.

Nevertheless, it is conceivable that this contamination could play a role, especially for the most disk-dominated objects. A precision measurement of this contribution will have to wait for high spatial resolution integral field spectroscopy, however we can get a sense of this effect by exploiting the available HST images. In fact, inclination plays a major role in determining the contribution of rotation to the unresolved line width. For a face on-disk, rotation does not contribute to the line width and therefore disk contamination is expected to bias towards lower stellar velocity dispersion of the bulge. For an edge-on disk, the unresolved velocity profile of the disk has width comparable to the stellar velocity dispersion of the bulge because they are contrasting the same potential[7] and therefore we could expect a smaller effect, or even an increase in velocity dispersion. For intermediate inclination objects, or for objects with no evidence of a disk – hereafter the intermediate/undefined sample – we can assume that disk contamination should introduce no bias in the velocity dispersion.

Fig. 11 shows the $M_{BH} - \sigma$ relation by color-coded inclination from our analysis on HST images (Paper II). Face-on spiral galaxies are shown as blue triangles, edge-on spirals are shown as open circles, the intermediate and /undefined sample is shown as solid circles. A galaxy, for which HST image is not available, is shown as a black square.

As expected, for a given BH mass, face-on spiral galaxies have lower velocity dispersion than edge-on and intermediate/undefined galaxies. Thus, it is possible that velocity dispersion of face-on galaxies are affected by cool stars with low velocity. If we exclude face on galaxies, the offset is found to be 0.45 ± 0.10 in BH mass (0.92 ± 0.10 and 0.43 ± 0.12, respectively for face-on and intermediate / undefined galaxies), 0.17 dex smaller than that of the total sample. It is remarkable that even the edge-on sample shows an offset in the same direction as the total sample. The intermediate/undefined sample in particular should be the cleanest with respect to disk contamination and still shows an offset from the local relationship, although of course the error bar is larger due to the much reduced sample size.

We conclude that disk contamination could reduce the offset by 0.17 dex, but not eliminate it.

6.2. *Are BH masses overestimated?*

6.2.1. *Is Hβ width overestimated?*

We estimate BH masses using the width of Hβ line and optical luminosity at 5100Å from single-epoch spectra, rather than the RMS spectra used in the derivation of the radius-luminosity relation for the reverberation sample (Peterson et al. 2004; Kaspi et al. 2005). Thus, we have to test whether our Hβ width measurement from single-epoch spectra is consistent with that from the RMS spectra.

In order to perform this test, we collected spectra for as many as possible of the objects in the reverberation sample of Onken et al. 2004 (our local calibrators). Specifically, we obtained single-epoch spectra for 6 Seyfert galaxies from International AGN Watch website[8]. Sin-

[7] For example, modeling the disk as an exponential (Freeman 1970) and the bulge as an $r^{1/4}$ (de Vaucouleurs 1948) profile, for an aperture equal to twice the effective radius and to twice the exponential length, the ratio between the second moment of the line of sight velocity and the velocity dispersion is ~ 0.86.

[8] URL http://www-astronomy.mps.ohio-state.edu/∼agnwatch

gle epoch spectra for 3 additional Seyfert galaxies were kindly provided by Aaron Barth, while mean spectra for 5 Seyfert galaxies were kindly provided by Bradley Peterson.

Fig. 12 compares for the 14 objects reverberation masses (Peterson et al. 2004; Onken et al. 2004) with our own BH mass estimates. To simplify the test, we adopted L_{5100} from Peterson et al. (2004), so that any discrepancy is only due to the difference between Hβ width from the RMS spectra and that from single-epoch (for 9 objects) or mean (for 5 objects) spectra. The reverberation masses are only slightly higher with a mean difference of 0.09 ± 0.07 dex (0.05 ± 0.11 and 0.16 ± 0.03, respectively for the single-epoch sample and the mean spectra sample), suggesting our Hβ measurements are consistent with reverberation results. This scatter and offset also provide an upper limit to possible systematics due to minor differences between our implementation of the algorithm for measuring the second moment of Hβ line width and that used by Peterson et al. (2004), including possible residual Fe II emission underneath the broad Hβ. We conclude that we do not find any evidence for systematic overestimation of Hβ width.

6.2.2. L_{5100} *overestimated?*

A potential concern is that L_{5100} could be overestimated if the host galaxy contribution is not negligible. However, the stellar component is not removed for the local calibration of the R_{BLR}-L_{5100} relation based on the reverberation mapped sample (Kaspi et al. 2005). Therefore, for consistency with their procedure we do not attempt such a removal. Future work on the analysis of HST images for our sample (Paper II) and for the local reverberation mapping sample (GO-10516, PI Peterson) will improve on this point.

Overall, given the slow dependence of the BH mass on L_{5100}, we expect any differences to be small. For example, if we suffered from *double* the amount of contamination by stellar light than that for the sample of local calibrators, the BH mass would be reduced by 0.1 dex, significantly smaller than the measured offset of 0.62 dex. Similarly, AGN variability at the expected level of $\lesssim$20-30% (i.e $\lesssim$0.05-0.08 dex) is a negligible effect (Webb & Malkan 2000) and its effect is already included in the overall estimate of the uncertainty of the BH mass from single-epoch data.

6.2.3. *BH mass 'shape' factor*

As mentioned previously, the geometry and kinematics of the broad-line clouds – which connect the observed broad line profile to the BH mass as $M_{BH} = f \times (\sigma^2_{H\beta}\ R_{BLR}/G)$, where R_{BLR} is the distance to the broad-line clouds, $\sigma_{H\beta}$ is the second moment of the Hβ line profile, and f is the shape factor – are not well constrained. A common practice in the literature is to adopt the shape factor expected for an isotropic distribution (i.e. f=3). Here, we adopt the recent Onken et al. (2004) shape factor, f=5.5, calibrated to fit the local $M_{BH} - \sigma$ relation using 14 Seyfert galaxies with measured stellar velocity dispersion and reverberation mass (see also Greene & Ho 2005b).

Although we adopt this new calibration of the shape factor, the evolution of the $M_{BH} - \sigma$ relation is *independent* of its numeric value – as long as it is constant with redshift – since the relative offsets among three redshift points in Fig. 9 are effectively BH mass ratios. If the assumption of constant shape factor is dropped, many different interpretations of our result become possible, including that the $M_{BH} - \sigma$ relation is constant but the shape factor evolves by a factor of four between $z = 0.36$ and today.

Unfortunately, direct measurement of BH masses around active galaxies at high-redshift are unlikely to become available in the near future, and therefore the shape factor cannot be directly determined for the moment. However, we note that the local Onken et al. sample is similar to our own in terms of BH mass, orientation (i.e. both are Seyfert 1s), and accretion rate (Woo & Urry 2002; see below). Therefore if these are the main parameters driving the geometry, their shape factor should be the same, at least on average. For this reason, we will continue in our discussion assuming that the shape factor is constant, but the reader is cautioned to keep this caveat in mind.

6.3. *Are these BHs growing rapidly?*

A final check concerns the mass accretion rate of the BHs. In fact, if the BHs were rapidly growing, this would need to be taken into account when comparing with the local relationship. For example, if the local relationship is the final destiny of our sample, velocity dispersions would need to grow more than 40% in the next 4 Gyrs to compensate for the increased mass.

The Eddington ratios are shown in Fig. 13, with the the Eddington Luminosity, defined as $L_{EDD} = 1.25 \times 10^{38}$ $M_{BH}/M_{\odot}$erg s^{-1}. As usual, bolometric luminosity is obtained as $9 \times L_{5100}$ (Peterson et al. 2004; adopting the larger bolometric correction suggested by Marconi et al. 2004 would not change our conclusions.) It is clear that our Seyferts typically have less than 10% of Eddington luminosity. Their mass accretion rates are in the range 0.3–0.7 $M_{\odot}$yr^{-1} assuming a standard 10% efficiency. For a typical AGN life time of < 0.1 Gyr (Martini 2004 and references therein), these BHs can grow at most by a factor of ~ 2, i.e. 0.3 dex. This amount of growth would strengthen the case for evolution in the velocity dispersion, implying that velocity dispersions would need to increase by $\sim$70 % in the next 4 Gyrs to conform to the local relationship.

7. DISCUSSION

In this section we interprets our results in terms of the co-evolution of spheroids and BHs. We consider three possible explanations for our results, ranked from the most prosaic to the most radical.

1) Systematic Errors. So far as the first explanation is concerned, in the previous section we discussed in detail a number of possible systematic uncertainties, and we could not find any single component large enough to bring our points in agreement with the Onken et al. points. It is possible that one or more of these sources of uncertainty are combining to enhance our measured evolution, but we consider it unlikely that the entire effect is due to a conspiracy of these sources of error (summing all the possible contributions listed in § 6, we estimate that the total systematic uncertainty is 0.25 dex in BH mass).

Another option is that the ECPI BH masses are less

accurate than expected, and possibly biased, depending on some still unknown additional parameters other than the Hβ width and L_{5100}. The tightness of our measured relation and other independent tests (e.g. Greene & Ho 2005b) are quite encouraging in this respect, but not yet conclusive. While we will continue our effort to increase the quality of our measurement in the distant universe, it is clear that much work remains to be done in the local universe. The sample of reverberation mapped AGNs used as local calibrators is still remarkably small, and covers a very limited range in fundamental parameters, such as BH mass, eddington ratio, orientation, etc.

2) Selection Effects. As the second explanation, selection effects also range from the trivial to the profound. Signal-to-noise ratio requirements introduce a minimum threshold in luminosity. Therefore, if there were a distribution of luminosities for any given BH mass, we would tend to bias towards the largest masses via Eq. 2. We made some progress in this respect, increasing our completeness from 7/13 (54%) to 14/20 (70%) between our pilot study and the present one. We also have a selection effect against strong Fe II emission, since that complicates stellar velocity dispersion measurements. It has been speculated that Fe II correlates with high accretion rate (Boroson & Green 1992), so excluding Fe II emitters could bias us against fastly growing and hence possibly smaller BHs. For the same reason, local studies tend to use the near infrared Ca II triplet for stellar kinematics. Systematic differences between Mgb + Fe and Ca II triplet kinematics could simulate an evolutionary trend, although they are unlikely to be as large as 0.15 dex (see Barth et al. 2003; Greene & Ho 2005c). We plan to increase our completeness and compare Mgb + Fe and Ca II triplet kinematics via optical and infrared spectroscopy in the near future.

At a more profound level, the local fundamental benchmark – the M_{BH}-σ relation – is based on only ~ 30 quiescent objects (e.g. Tremaine et al. 2002), most of them elliptical and lenticular galaxies – i.e. collisionless and dynamically relaxed systems, except for 4 spirals (MW, M31, NGC1068, and NGC4258). Selection effects could be at work to artificially tighten the relationship. It is plausible to imagine a scenario where the M_{BH}-σ relation is an evolutionary endpoint, rather than a time invariant property of all galaxies. For example, it is possible that only after a sufficient long time the amount of baryons that has been converted into stars – which mergers have relocated from the disk to the bulge – and the amount of baryons accreted by the central BH, will be constant fractions of the total amount available, and thus proportional to each other. However, the road to the M_{BH}-σ relation could be full of traumatic events such as gas-rich mergers, and during their life time galaxies could have roamed through the M_{BH}-σ plane (e.g. Kazantzidis et al. 2005). If we only measured the relation for well-behaved early-type galaxies – where stellar orbits are easy to measure and to model – we could artificially select the objects in their tight final correlation. If points on the M_{BH}-σ diagram were selected by their BH mass – as opposed to by the mass of the spheroid – we could imagine to find objects that lie above the end-point relation, if they existed. Since our sample is effectively selected for having a massive BH, a selection effect of this sort could provide an explanation of our findings that is still in some sense "evolutionary". In this respect, once again, the local samples of AGNs play a crucial role, being selected for their BH rather than for their bulge. By comparing our objects with the AGNs selected sample of Onken et al. (2004) – instead of the Tremaine et al. (2002) quiescent sample – we are minimizing this sort of selection effect. Ongoing work to extend the sample of AGNs with reverberation mapping BH masses (Peterson, 2005, private communication) and to obtain direct mass measurements for some of the same objects (Hicks 2005) is extremely important to improve the determination of the local M_{BH}-σ relation and its scatter. Recent results could indicate that the relationship could have more scatter than imagined, especially at smaller masses (Peterson et al. 2005).

3) Cosmic Evolution. This is probably the most surprising at first, given that the last 4 Gyrs are in many respects a rather quiet phase of the life of the universe (consider, e.g., the sharp decline of the cosmic star formation rate since $z \sim 1$, Lilly et al. 1995). However, evolution has been observed in the galaxy population, at least at masses comparable to those of the galaxies in our sample. In the velocity dispersion range covered by our sample, significant evolution and star formation is seen even in early-type galaxies (Treu et al. 2005a,b; van der Wel et al. 2005; di Serego Alighieri et al. 2005). There is evidence that the morphological mix changed significantly in last $\sim$5 Gyr, both in the field (Bundy et al. 2005) and in clusters (Dressler et al. 1997). As far as AGN hosts are concerned, recent studies show that the hosts of the most massive BHs have relatively old stellar populations, perhaps as old as those of massive quiescent ellipticals (Woo et al. 2004, 2005), but little is known for smaller mass systems. If evolution were found to be much more recent for smaller mass system, this could be an indication of 'downsizing' (Cowie et al. 1996; Treu et al. 2005a) for AGN-hosts as well. General arguments have been given suggesting that the global accretion and star-formation history of the Universe and the growth of bulges follow the growth of supermassive BHs (Merloni et al. 2004).

More specifically, the real test of our result is provided by independent measures of the M_{BH}-σ relation. Shields et al. (2003) combines an [O III]-based estimate of the velocity dispersion with ECPI estimates of the BH mass to find a result consistent with no evolution out to $z \sim 3$. However, the scatter of their measurement (i.e. ~ 0.5 dex in the offset from the $M_{BH} - \sigma$ relation) could soften the evolutionary constraints imposed on the relation. Furthermore, as discussed in Section 3.3, for high(low)-luminosity quasars of Shields et al. sample, stellar velocity dispersion could be over(under)estimated since [O III] line widths are systematically larger(smaller) than stellar velocity dispersion with an increasing(decreasing) function of Eddington ratio (Greene & Ho 2005a), possibly diluting any signature of evolution. Furthermore, the mass and redshift range is completely different from our own, making it even harder to compare the two measurements. Walter et al. (2004) combines CO-based velocity dispersion with an ECPI based mass estimate for a system at $z \sim 6$, and finds evolution in the same sense as we do, although certainly this study is more comparable to that of Shields et al. (2003) in terms of mass and redshift range. Another test is provided by studies of the relationship between BH mass and host galaxy luminosity or

stellar mass for distant galaxies, which also find evidence for AGNs with smaller bulges than expected (Magain et al. 2005; Peng et al. 2005).

One rationalization of our observations is that most galaxies are formed as a blue, star-forming, disk or irregular state and that this phase is terminated by a major merger. The consequences of this merger are threefold. Firstly, there will be an onset of nuclear activity as gas, either present in the major partner or contributed by the minor partner, is driven into the accretion disk orbiting the major BH. This creates the Type I Seyfert galaxies in the state, as we observe them in our sample, where the mass supply rate is significantly lower than the Eddington rate.

Secondly, the mass supply builds up to exceed the Eddington rate and this leads to a powerful, disk-driven outflow which expels cool, interstellar gas (Silk & Rees 1998, Blandford 1999), and brings about the transition from the blue sequence to the red sequence, which has been postulated by Hopkins et al. (2006) to occur at a characteristic mass which increases with redshift. In the model of Hopkins et al., the estimated transition stellar mass at $z = 0.36$ is $\sim 3 \times 10^{10} M_{\odot}$. This is consistent within the stellar luminosity of the galaxies in our sample (we will revisit this point in Paper II). Normally, dry mergers of spheroids do not change the velocity dispersion (Nipoti et al. 2003 and references therein; but see Boylan-Kolchin et al. 2006 for more general results). However, it is our conjecture that the combination of gas dynamical interaction between interstellar molecular clouds and an outflowing wind, as a short-lived dynamical phase, will lead to some dissipation within the stars and a consequent increase in the velocity dispersion. In addition, the direct transfer of stellar mass from the disk component of the merging galaxies to the spheroids could further boost the final bulge mass (Croton 2006) and hence its velocity dispersion.

The third phase may occur considerably later and involves three body interactions of three or more merging BHs in the center of the combined galaxy. This can lead to the ejection of some of the BH mass (e.g. Favata et al. 2004, Blanchet et al. 2005, Haehnelt, Davis & Rees 2006, Hoffmann & Loeb 2006), further lowering the $M_{BH} - \sigma$ relation.

In conclusion, it appears that – at least qualitatively – dissipational mergers must play an important role in the later stages of assembly of spheroidals (see also Nipoti et al. 2003; Kazantzidis et al. 2005; Roberston et al. 2005; Treu et al. 2006; Koopmans et al. 2006) if evolution is the correct interpretation of our observations.

8. SUMMARY

We summarize our results as follows:

1) We test the evolution of the $M_{BH} - \sigma$ relation, by measuring stellar velocity dispersions with high S/N spectra for a sample of 14 Seyfert 1 galaxies at $z = 0.36 \pm 0.01$. BH masses are estimated using the Hβ line width and the optical luminosity at 5100Å, based on the empirically-calibrated photo-ionization method.

2) We find a significant offset, $\Delta \log M_{BH} = 0.62 \pm 0.10$ ($\Delta \log \sigma = 0.15 \pm 0.03$) from the local relation of Tremaine et al. (2002), and $\Delta \log M_{BH} = 0.57 \pm 0.11$ ($\Delta \log \sigma = 0.14 \pm 0.03$) from that of Ferrarese (2002), in the sense that velocity dispersions were smaller for given BH masses at this redshift.

3) We investigate various sources of systematic errors, and find that those cannot account for the observed offset. Combining systematic errors of aperture correction (<0.15 dex in M_{BH}), contamination from cold disk kinematics (0.17 dex), and stellar contamination to the optical luminosity at 5100Å (0.1 dex), we estimate an upper limit to the systematic uncertainty of 0.25 dex in BH mass (0.06 in $\Delta \log \sigma$).

4) Along with two samples of AGNs at lower redshifts, we quantify the observed evolution with the best fit linear relation, $\Delta \log M_{BH} = (1.66 \pm 0.43) z + (0.04 \pm 0.09)$ with respect to Tremaine et al. (2002), and $\Delta \log M_{BH} = (1.55 \pm 0.46) z + (0.01 \pm 0.12)$ with respect to Ferrarese (2002), consistent with the scenario where the BH growth predates bulge assembly at these mass scales (σ=120–220 km s^{-1}).

5) We compare three measurements of the [O III] λ5007 line widths with the stellar velocity dispersions and find a scatter of ∼25% (i.e 0.1 dex in σ, or 0.4 dex in M_{BH}), and systematic offsets depending on the line fitting methods. These uncertainties must be accounted for when studying the evolution of the $M_{BH} - \sigma$ relation, especially with a small sample.

In § 7 we discussed three possible explanations for the observed offset: 1) systematic errors; 2) selection effects; 3) cosmic evolution. Systematic errors are unlikely to account for the offset (∼0.60 dex), which is significantly larger than the overall systematic uncertainty (0.25 dex). Selection effects could be present both in our sample (selected against low luminosity AGNs and thus small BH masses), and in the local sample (favoring more evolved systems), possibly resulting in the observed evolution of the $M_{BH} - \sigma$ relation. In order to minimize selection effects, we compared our z=0.36 galaxies to the sample of local AGNs from the study of Onken et al. (2004). The two samples are well matched in terms of host galaxy morphology, suggesting that morphological selection effects are not the dominant component. However, larger samples of AGNs with determined BH mass, stellar velocity dispersion, and host galaxy morphology are needed both locally and at high-redshift to improve the understanding of selection effects. Finally, if cosmic evolution is the correct explanation, the observed offset would support earlier growths of supermassive BHs in galaxies with mass scales of $\langle\sigma\rangle$=170 km s^{-1}. This could be evidence for 'downsizing' in the BH-galaxy coevolution i.e. more massive galaxies arrive at the local relationship early in time. This scenario can be further investigated with a sample of AGN host galaxies with a range in mass at fixed redshifts.

We thank the referee for useful suggestions. We thank Todd Boroson for providing the I Zw 1 Fe II template; Brad Peterson and Marianne Vestergaard for useful suggestions and for sending us the RMS and mean spectra of several local Seyfert galaxies with measured reverberation BH masses; Aaron Barth for numerous stimulating conversations and for providing us with high S/N Palomar/Hale spectra of 3 Seyfert galaxies. We acknowledge stimulating conversations with Peng Oh, Robert (Ski) Antonucci, and Giovanni Fossati. This work is based on data collected at Keck Observatory – operated by Cal-

tech and the University of California – and with the Hubble Space Telescope operated by AURA under contract from NASA. This project is made possible by the wonderful public archive of the Sloan Digital Sky Survey. We acknowledge financial support by NASA through HST grant GO-10216.

REFERENCES

Barth, A., Ho, L., & Sargent, W. L. W. 2002, ApJ, 566, L13
Barth, A. J., Ho, L. C., & Sargent, W. L. W. 2003, ApJ, 583, 134
Barth, A. J., Greene, J. E., & Ho, L. C. 2005, ApJ, 619, L151
Bell, E. F., et al. 2005, ApJ, 625, 23
Blanchet, L., Qusailah, M. S. S., & Will, C. M. 2005, ApJ, 635, 508
Blandford, R. D., & McKee, C. F. 1982, ApJ, 255, 419
Blandford, R. D. 1999, Galaxy Dynamics ed. D. Merritt, M. Valluri, and J. Sellwood San Francisco: ASP p.87
Blumenthal, G. R., Faber, S. M., Primack, J. R., & Rees, M. J. 1984, Nature, 311, 517
Boroson, T. A., & Green, R. F. 1992, ApJS, 80, 109
Boroson, T. A. 2003, ApJ, 585, 647
Boroson, T. 2005, AJ, 130, 381
Bonning, E. W., Shields, G. A., Salviander, S., & McLure, R. J. 2005, ApJ, 626, 89
Boylan-Kolchin, M., Ma, C.-P., Quataert, E. 2004, ApJ, 613, L37
Boylan-Kolchin, M., Ma, C.-P., Quataert, E. 2006, MNRAS, submitted (astro-ph/0601400)
Brotherton, M. S. 1996, ApJS, 102, 1
Bundy, K., Ellis, R. S., & Conselice, C. J. 2005, ApJ, in press
Cattaneo, A., Blaizot, J., Devriendt, J., & Guiderdoni, B. 2005, MNRAS, 364, 407
Ciotti, L., & van Albada, T. S. 2001, ApJ, 552, L13
Cowie, L. L., Songaila, A., Hu, E. M., & Cohen J. G. 1996, AJ, 112, 839
Croton, D. J., et al. 2006, MNRAS, 365, 11
Croton, D. J. 2005, MNRAS, sumbitted (astro-ph/0512375)
Dalla Vecchia, C., Bower, R. G., Theuns, T., Balogh, M. L., Mazzotta, P., & Frenk, C. S. 2004, MNRAS, 355, 995
De Lucia, G., Springel, V., White, S. D. M., Croton, D., & Kauffmann, G. 2006, MNRAS, 366, 499
di Serego Alighieri, S., et al. 2005, A&A, 442, 125
Djorgovski, S., & Davis, M. 1987, ApJ, 313, 59
Dressler, A., Lynden-Bell, D., Burstein, D., Davies, R. L., Faber, S. M., Terlevich, R., & Wegner, G. 1987, ApJ, 313, 42
Dressler, A., et al. 1997, ApJ, 490, 577
Favata, M., Hughes, S. A., & Holz, D. E. 2004, ApJ, 607, L5
Ferrarese, L., & Merritt, D. 2000, ApJ, 539, L9
Ferrarese, L. 2002, Current high-energy emission around black holes, 3
Graham, A. 2004, ApJ, 613, L33
Gebhardt, K., et al. 2000, ApJ, 539, L13
Greenee, J. E. & Ho, L. 2005a, ApJ, 627, 721
Greene, J. E., & Ho, L. C. 2005b, ArXiv Astrophysics e-prints, arXiv:astro-ph/0512461
Greene, J. E., & Ho, L. C. 2005c, ArXiv Astrophysics e-prints, arXiv:astro-ph/0512462
Haehnelt, M. G., Davies, M. B., & Rees, M. J. 2006, MNRAS, 366, L22
Häring, N., & Rix, H.-W. 2004, ApJ, 604, L89
Heckman, T. M., Kauffmann, G., Brinchmann, J., Charlot, S., Tremonti, C., & White, S. D. M. 2004, ApJ, 613, 109
Hicks, E. 2005, BAAS, 207, 5602
Hoffman, L., & Loeb, A. 2006, ApJL, in press
Hopkins, P. F., Bundy, K., Hernquist, L., & Ellis, R. S. 2006, ApJL, submitted, ArXiv Astrophysics e-prints, arXiv:astro-ph/0601621
Hunt, L. K., & Malkan, M. A. 2004, ApJ, 616, 707
Hunt, L. K. et al.1997, ApJS, 108, 229
Hunt, L. K., Malkan, M. A., Moriondo, G., & Salvati, M. 1999, ApJ, 510, 637
Jørgensen, I., Franx, M., & Kjærgaard, P. 1995, MNRAS, 276, 1341
Juneau, S., et al. 2005, ApJ, 619, L135
Kaspi, S., Smith, P. S., Netzer, H., Maoz, D., Jannuzi, B. T., & Giveon, U. 2000, ApJ, 533, 631
Kaspi, S., Maoz, D., Netzer, H., Peterson, B. M., Vestergaard, M., & Jannuzi, B. T. 2005, ApJ, 629, 61
Kauffmann, G., & Haehnelt, M. 2000, MNRAS, 311, 576
Kazantzidis, S., et al. 2005, ApJ, 623, L67
Koopmans, L. V. E., et al. 2006, ApJ, submitted (astro-ph/0601628)
Lilly, S. J., Tresse, L., Hammer, F., Crampton, D., & Le Fevre, O. 1995, ApJ, 455, 108
Magain, P., Letawe, G., Courbin, F., Jablonka, P., Jahnke, K., Meylan, G., & Wisotzki, L. 2005, Nature, 437, 381
Magorrian, J., et al. 1998, AJ, 115, 2285
Marconi, A., & Hunt, L. K. 2003, ApJ, 589, L21
Marconi, A., Risaliti, G., Gilli, R., Hunt, L. K., Maiolino, R., & Salvati, M. 2004, MNRAS, 351, 169
Martini, P. 2004, Coevolution of Black Holes and Galaxies, 169
Marziani, P., Sulentic, J. W., Zamanov, R., Calvani, M., Dultzin-Hacyan, D., Bachev, R., & Zwitter, T. 2003, ApJS, 145, 199
McLure, R. J., & Dunlop, J. S. 2002, MNRAS, 331, 795
Menci, N., Cavaliere, A., Fontana, A., Giallongo, E., Poli, F., & Vittorini, V. 2003, ApJ, 587, L63
Merloni, A. 2004, MNRAS, 353, 1035
Merloni, A., Rudnick, G., & Di Matteo, T. 2004, MNRAS, 354, L37
Milosavljevic, M., Merrit, D., Rest, A., van den Bosch, F.C. 2002, MNRAS, 331, L51
Miralda-Escudé, J., & Kollmeier, J. A. 2005, ApJ, 619, 30
Nelson, C. H., & Whittle, M. 1996, ApJ, 465, 96
Nelson, C. H., Green, R. F., Bower, G., Gebhardt, K., & Weistrop, D. 2004, ApJ, 615, 652
Nipoti, C., Londrillo, P., & Ciotti, L. 2003, MNRAS, 342, 501
Novak, G. S., Faber, S. M., & Dekel, A. 2006, ApJ, 637, 96
Onken, C. A., Ferrarese, L., Merritt, D., Peterson, B. M., Pogge, R. W., Vestergaard, M., & Wandel, A. 2004, ApJ, 615, 645
Padmanabhan, N., et al. 2004, New Astronomy, 9, 329
Peng, C. Y., Impey, C. D., Ho, L. C., Barton, E. J., & Rix, H.-W. 2005, ApJ, accepted
Peterson, B. M. 1993, PASP, 105, 247
Peterson, B. M., et al. 2004, ApJ, 613, 682
Peterson, B. M., et al. 2005, ApJ, 632, 799
Pizzella, A., Corsini, E. M., Vega Beltrán, J. C., & Bertola, F. 2004, A&A, 424, 447
Rix, H.-W., & White, S. D. M. 1992, MNRAS, 254, 389
Robertson, B., et al. 2005, ApJ, in press (astro-ph/0506038)
Rosenblatt, E. I., Malkan, M. A., Sargent, W. L. W., & Readhead, A. C. S. 1994, ApJS, 93, 73
Salucci, P., Szuszkiewicz, E., Monaco, P., & Danese, L. 1999, MNRAS, 307, 637
Shankar, F., Salucci, P., Granato, G. L., De Zotti, G., & Danese, L. 2004, MNRAS, 354, 1020
Shields, G. A., Gebhardt, K., Salviander, S., Wills, B. J., Xie, B., Brotherton, M. S., Yuan, J., & Dietrich, M. 2003, ApJ, 583, 124
Silk, J., & Rees, M. J. 1998, A&A, 331, L1
Small, T. A., & Blandford, R. D. 1992, MNRAS, 259, 725
Soltan, A. 1982, MNRAS, 200, 115
Stiavelli, M. 1998, ApJ, 495, L91
Springel, V., Di Matteo, T., & Hernquist, L. 2005, MNRAS, 361, 776
Stocke, J. T., Morris, S. L., Gioia, I. M., Maccacaro, T., Schild, R., Wolter, A., Fleming, T. A., & Henry, J. P. 1991, ApJS, 76, 813
Tamura, N., Ohta, K., & Ueda, Y. 2006, MNRAS, 365, 134
Trager, S. C., Worthey, G., Faber, S. M., Burstein, D., & Gonzalez, J. J. 1998, ApJS, 116, 1
Trager, S. C., Faber, S. M., Worthey, G., & González, J. J. 2000, AJ, 119, 1645
Tremaine, S., et al. 2002, ApJ, 574, 740
Treu, T., Malkan, M., & Blandford, R. D. 2004, ApJ, 615, L97 (TMB04)
Treu, T., Ellis, R. S., Liao, T. X., & van Dokkum, P. G. 2005a, ApJ, 622, 5
Treu, T., et al. 2005b, 633, 174
Treu, T., et al. 2006, ApJ, in press
van der Marel, R. P. 1994, MNRAS, 270, 271
Vanden Berk, D. E., et al. 2001, AJ, 122, 549
van der Wel, A., Franx, M., van Dokkum, P. G., Rix, H.-W., Illingworth, G. D., & Rosati, P. 2005, ApJ, 631, 145
van Dokkum, P. G. 2001, PASP, 113, 1420
Vestergaard, M. 2002, ApJ, 571, 733

Vittorini, V., Shankar, F., & Cavaliere, A. 2005, MNRAS, 363, 1376
Volonteri, M., Haardt, F., & Madau, P. 2003, ApJ, 582, 559
Walter, F., Carilli, C., Bertoldi, F., Menten, K., Cox, P., Lo, K. Y., Fan, X., & Strauss, M. A. 2004, ApJ, 615, L17
Wandel, A., Peterson, B. M., & Malkan, M. A. 1999, ApJ, 526, 579
Webb, & Malkan, A. 2000, ApJ, 540, 652
White, S. D. M., & Rees, M. J. 1978, MNRAS, 183, 341
Willott, C. J., McLure, R. J., & Jarvis, M. J. 2003, ApJ, 587, L15
Woo, J.-H., & Urry, C. M. 2002, ApJ, 579, 530
Woo, J.-H., Urry, C. M., Lira, P., van der Marel, R. P., & Maza, J. 2004, ApJ, 617, 903
Woo, J.-H., Urry, C. M., van der Marel, R. P., Lira, P., & Maza, J. 2005, ApJ, 631, 762
Wyithe, J. S. B., & Loeb, A. 2005, ApJ, 634, 910
Yu, Q., & Tremaine, S. 2002, MNRAS, 335, 965

TABLE 1
Journal of observations

Run	Date	Grating line mm^{-1}	Slit Width arcsec	Seeing arcsec	Conditions
(1)	(2)	(3)	(4)	(5)	(6)
1	2003 Mar 6	900	1.5	∼1	cirrus
2	2003 Sep 3	900	1.5	∼1	cirrus
3	2004 May 14	900	1	∼1	cirrus
4	2004 May 22	831	1	∼0.8	clear
5	2005 Jul 7,8	900/831	1	0.7-0.9	clear

Note. — Col. (1): Observing run. Col. (2): Observing date. Col. (3): Grating. Col. (4): Slit width. Col. (5): Seeing FWHM. Col. (6): Conditions.

TABLE 2
Targets and Exposures

Name	z	RA (J2000)	DEC (J2000)	r'	Run	Exp.	S/N
(1)	(2)	(3)	(4)	(5)	(6)	(7)	(8)
S01	0.3596	15 39 16.23	+03 23 22.06	18.94	2,5	7200	69
S02	0.3544[1]	16 11 11.67	+51 31 31.12	18.94	2	3000	44
S03	0.3583[1]	17 32 03.11	+61 17 51.96	18.26	2	1800	55
S04	0.3580	21 02 11.51	-06 46 45.03	18.75	2	2400	47
S05	0.3531	21 04 51.85	-07 12 09.45	18.43	2,5	12600	111
S06	0.3689	21 20 34.19	-06 41 22.24	18.53	2	3000	31
S07	0.3520	23 09 46.14	+00 00 48.91	18.13	2,5	7200	100
S08	0.3591	23 59 53.44	-09 36 55.53	18.61	2	2400	54
S09	0.3548	00 59 16.11	+15 38 16.08	18.33	2	2700	39
S10	0.3506[1]	01 01 12.07	-09 45 00.76	17.91	2	600	52
S11	0.3562	01 07 15.97	-08 34 29.40	18.43	2,5	4800	110
S12	0.3575	02 13 40.60	+13 47 56.06	18.18	2	1800	38
S21	0.3534[1]	11 05 56.18	+03 12 43.26	17.50	3	1500	70
S23	0.3515	14 00 16.66	-01 08 22.19	18.22	3,5	5400	67
S24	0.3621	14 00 34.71	+00 47 33.48	18.43	3,5	9600	98
S26	0.3691	15 29 22.26	+59 28 54.56	18.93	3	7200	47
S27	0.3667[1]	15 36 51.28	+54 14 42.71	18.87	3	7200	41
S28	0.3682	16 11 56.30	+45 16 11.04	18.78	4,5	5760	73
S29	0.3575[1]	21 58 41.93	-01 15 00.33	18.87	4	3600	56
S99	0.3690	16 00 02.80	+41 30 27.00	18.78	1	4800	42

References. — a) redshift from SDSS DR4.

Note. — Col. (1): Target ID. Col. (2): Redshift from stellar absorption lines. Col. (3): RA. Col. (4): DEC. Col. (5): Extinction corrected r' AB magnitude from SDSS photometry. Col. (6): Observing run. Col. (7): Total exposure time in seconds. Col. (8): Signal-to-noise ratio per 0.85Å pixel of the combined spectrum (average in the 6900-7400Åspectral region).

TABLE 3
Observed and derived properties

Name	$\sigma_{H\beta}$ Å	$\sigma_{H\beta}$ km s^{-1}	f_{5100} 10^{-17} erg cm^{-2} Å^{-1} s^{-1}	λL_{5100} 10^{44} erg s^{-1}	log $M_{BH}/M_\odot$	σ km s^{-1}	Type
(1)	(2)	(3)	(4)	(5)	(6)	(7)	(8)
S01	46.6± 0.5	2116. ± 21.	5.83± 0.01	1.77± 0.01	8.20	132± 8	Sb
S02	43.7± 0.9	1992. ± 43.	5.35± 0.02	1.57± 0.01	8.11	-	E/S0
S03	41.2± 0.5	1872. ± 21.	10.77± 0.03	3.25± 0.01	8.28	-	Sb
S04	52.2± 0.6	2367. ± 29.	7.83± 0.02	2.38± 0.01	8.39	186± 8	Sa
S05	67.8± 0.7	3090. ± 33.	9.44± 0.00	2.74± 0.01	8.66	132± 5	Sb
S06	48.8± 0.9	2198. ± 43.	9.07± 0.01	2.95± 0.01	8.39	169± 14	Sb
S07	51.4± 0.5	2345. ± 24.	11.25± 0.01	3.23± 0.01	8.47	145± 13	Sc
S08	36.0± 0.6	1635. ± 26.	8.72± 0.02	2.63± 0.01	8.10	187± 11	Sa
S09	43.0± 0.3	1960. ± 16.	11.06± 0.02	3.23± 0.01	8.32	187± 15	M
S10	44.6± 0.4	2037. ± 18.	14.62± 0.04	4.18± 0.01	8.43	-	Sb
S11	40.1± 0.2	1822. ± 7.	9.23± 0.01	2.74± 0.00	8.20	127± 9	S0
S12	73.7± 0.1	3346. ± 5.	12.84± 0.02	3.87± 0.01	8.83	173± 22	Sb
S21	68.8± 0.5	3137. ± 22.	26.54± 0.46	7.73± 0.13	8.99	-	M
S23	73.3± 0.6	3345. ± 29.	12.10± 0.01	3.46± 0.01	8.80	172± 8	Sb
S24	61.6± 0.4	2792. ± 20.	9.96± 0.01	3.08± 0.01	8.61	214± 10	Sb
S26	41.6± 1.1	1871. ± 50.	4.97± 0.08	1.62± 0.03	8.07	128± 8	Sb
S27	38.9± 0.5	1754. ± 21.	6.18± 0.10	1.98± 0.03	8.07	-	M
S28	54.4± 0.4	2450. ± 17.	7.33± 0.01	2.37± 0.01	8.42	210± 10	
S29	45.0± 0.9	2044. ± 41.	6.16± 0.01	1.85± 0.01	8.18	-	
S99	70.9± 2.1	3196. ± 94.	8.02± 0.01	2.59± 0.01	8.67	224± 12	S0/a

Note. — Col. (1): AGN name. Col. (2): Second moment of Hβ in the observed frame. Col. (3): Second moment of Hβ in km s^{-1}. Following Peterson et al. (2004), FWHM can be obtained by multiplying a factor of 2.03 ± 0.59. Col. (4): Observed flux at 5100(1+z)Å, calibrated with SDSS photometry. Col. (5): Rest frame luminosity at 5100Å. Col. (6): Logarithm of BH mass in solar units. Estimated uncertainty is 0.4 dex (Vestgaard 2002). Col. (7): Stellar velocity dispersion with uncertainty. Col. (8): Host galaxy morphological type determined from HST imaging (Paper II). M identifies merging galaxies.

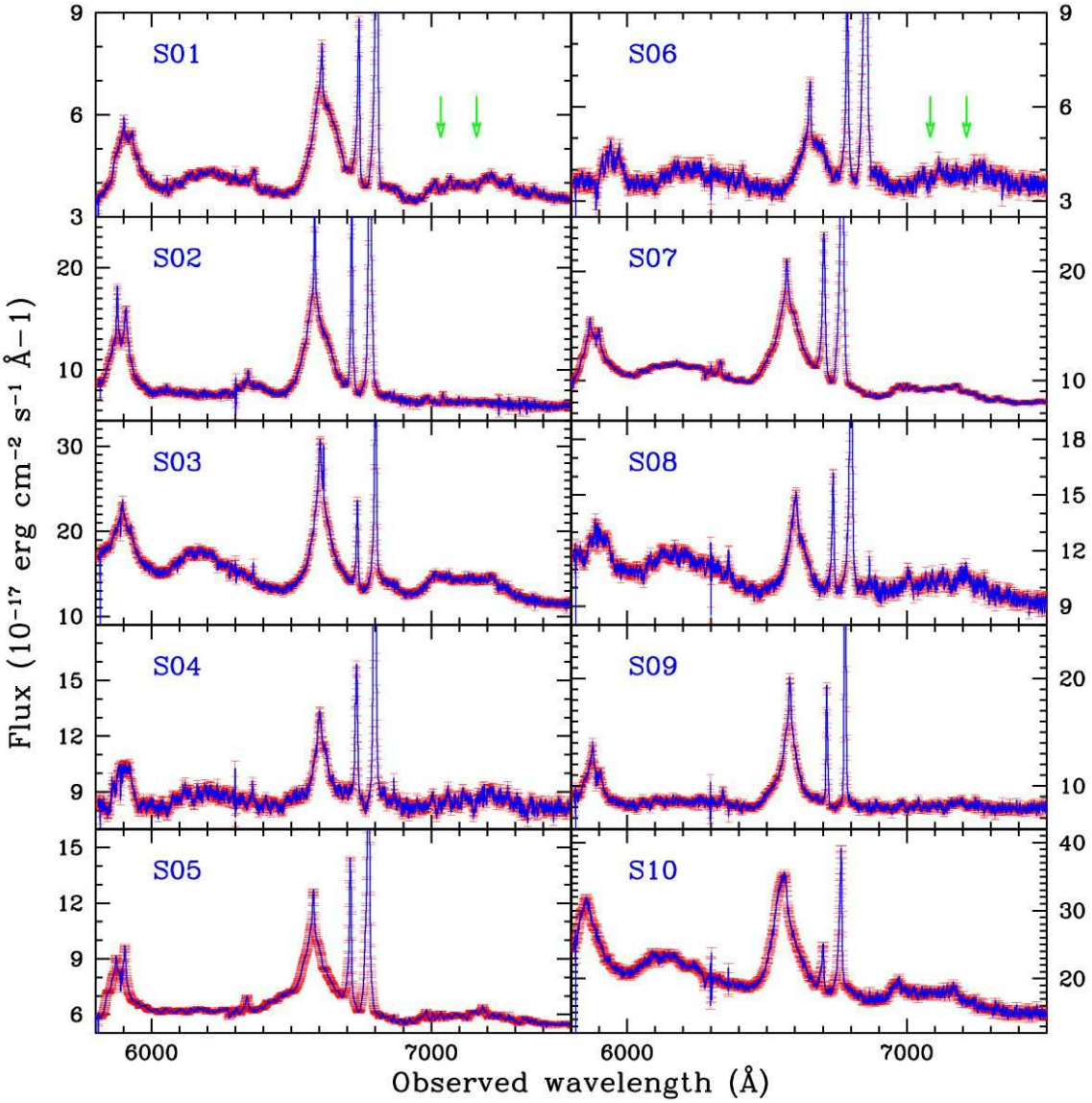

FIG. 1.— Flux calibrated Keck spectra of all 20 Seyfert 1 galaxies. Broad Hβ and [O III] lines are clearly present at the center of the wavelength range. In many cases, stellar absorption features are also visible redward of [O III]. The level of noise is indicated by the red error bars. Green arrows indicate the location of the stellar features, Mgb (5175 Å) and Fe (5270 Å).

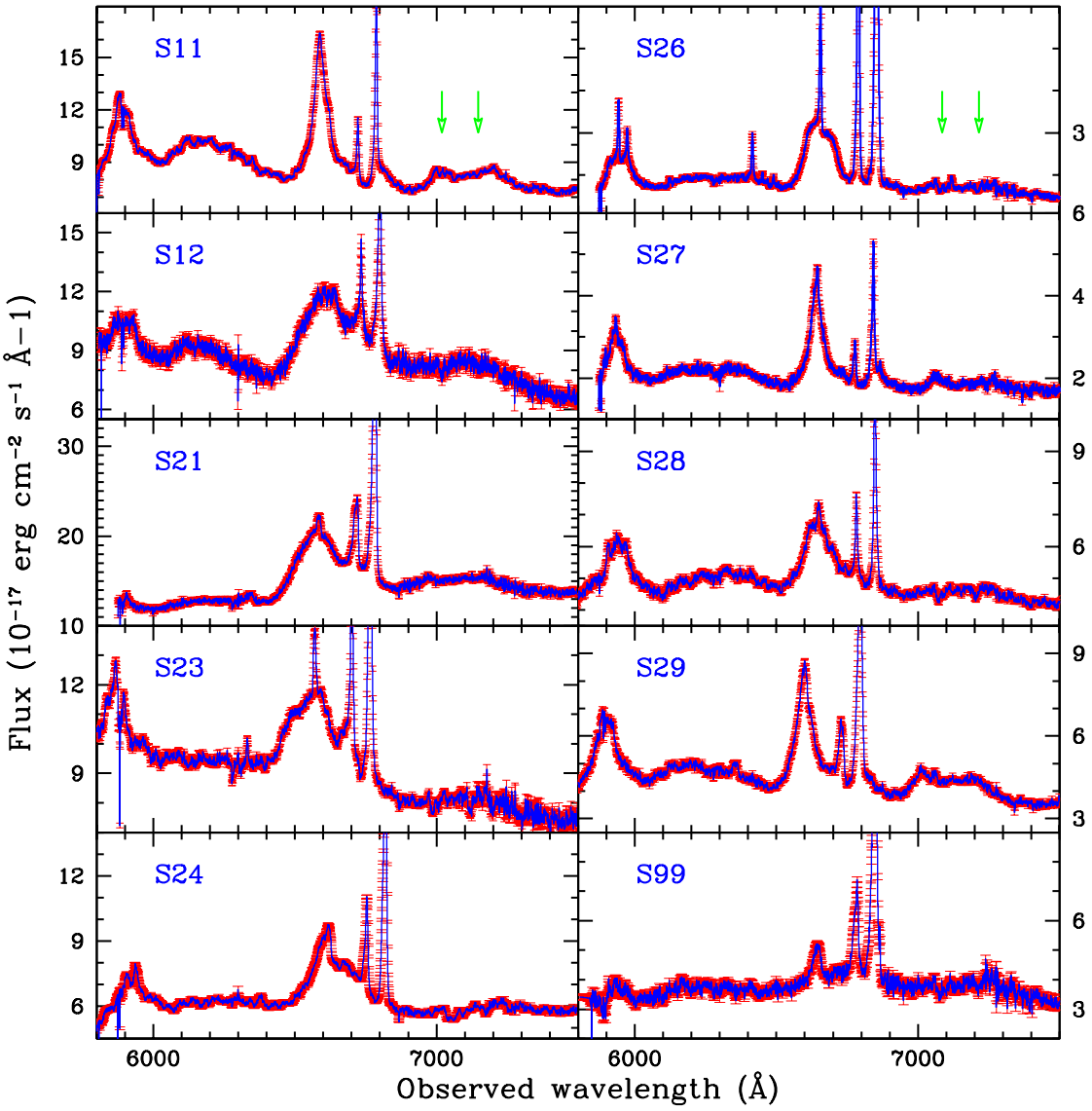

Fig. 1. — Continued.

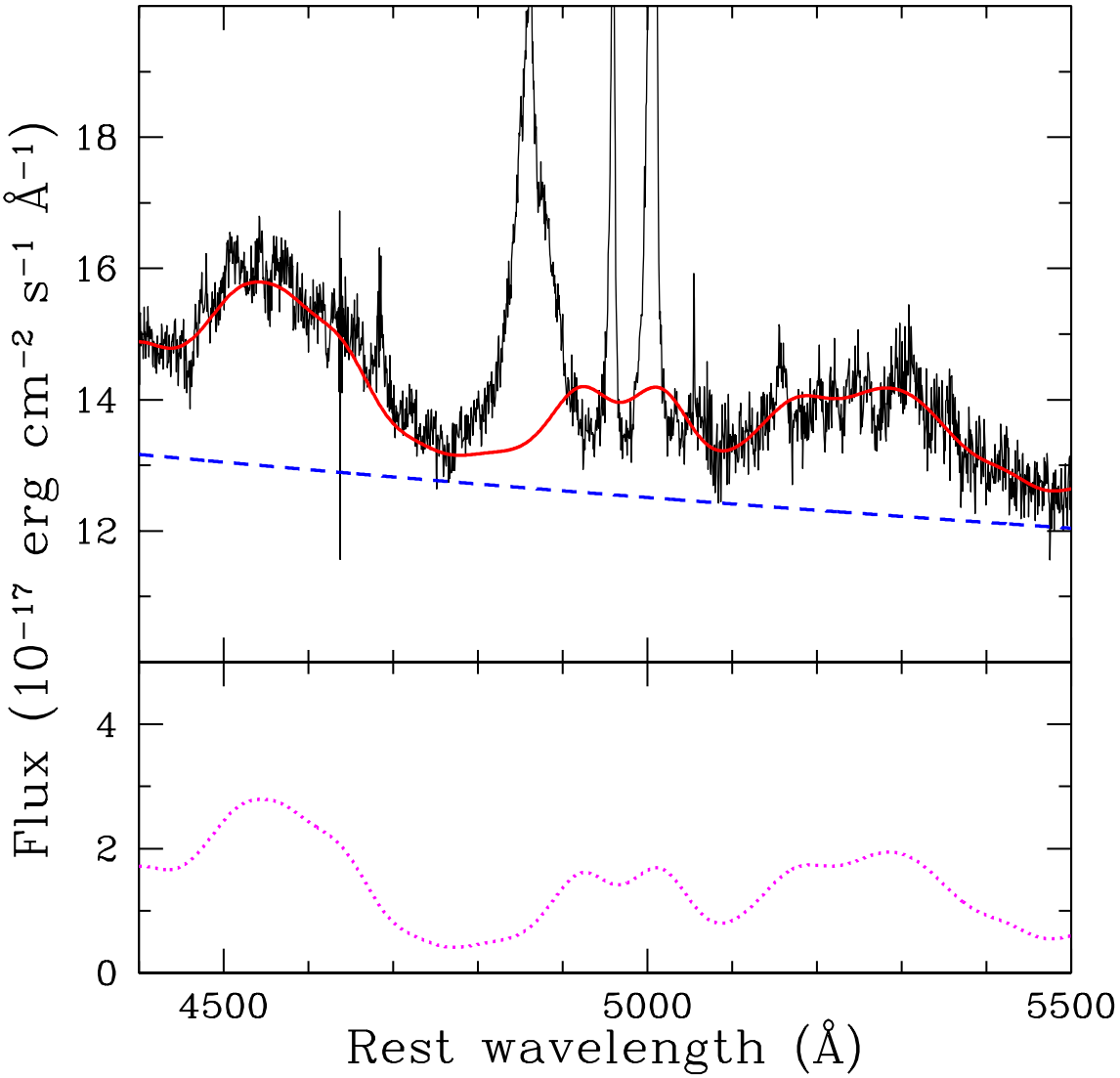

FIG. 2.— Example of broad Fe II emission fit with I Zw 1 template and a featureless continuum. The best fit model (solid *red* line; top panel), composed of a broadened Fe II template (dotted *magenta* line; lower panel) and AGN+stellar continuum (dashed *blue*; upper panel), is compared with the observed spectrum (*black* histogram; upper panel). Three free parameters, i.e. continuum slope, Fe II width, and Fe II strength are determined by minimizing the χ^2 in the spectral region 5100-5500 Å.

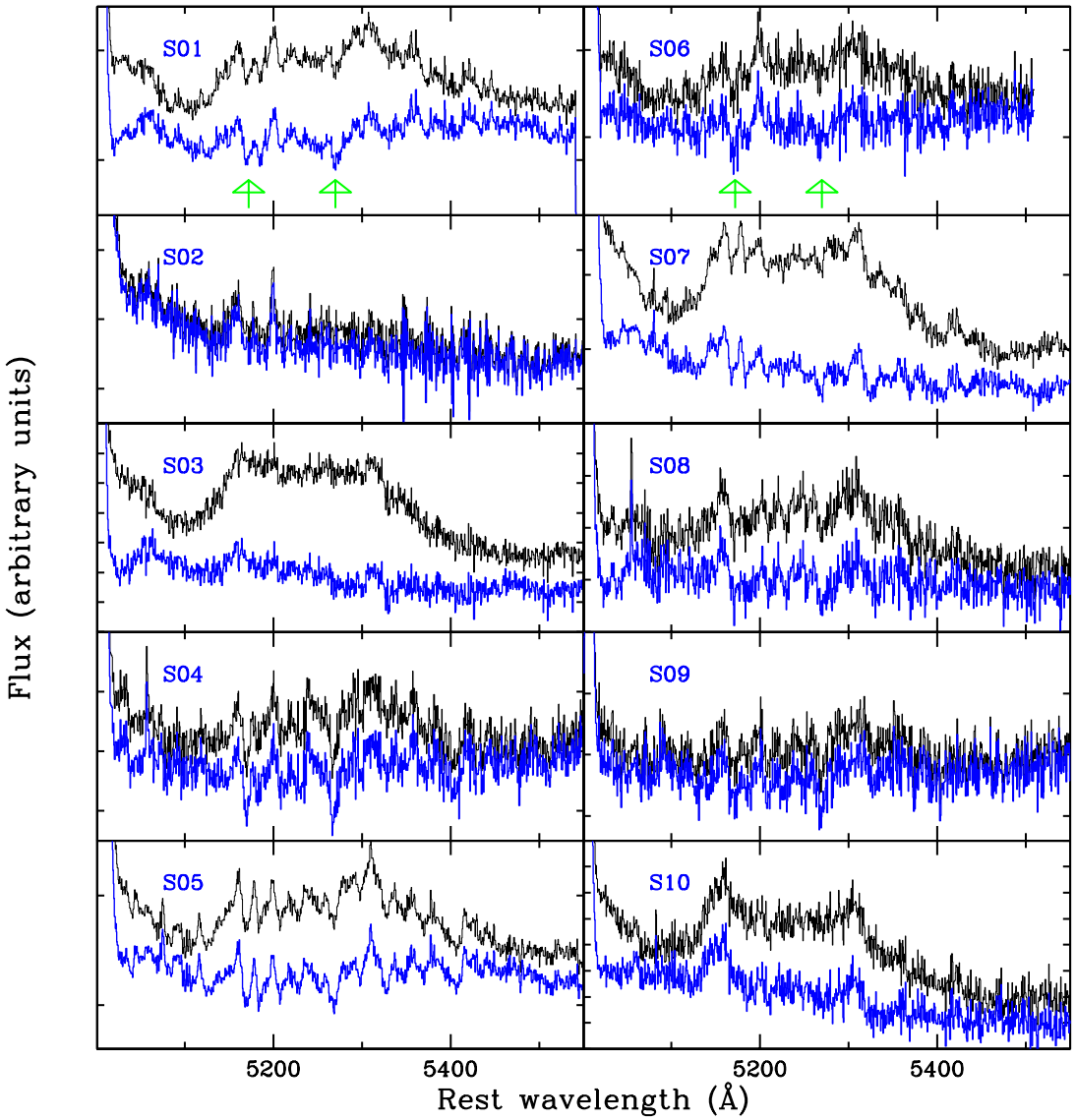

FIG. 3.— Rest frame spectra before (upper black histogram) and after (lower blue histogram) Fe II subtraction. Note the large range of Fe II emission strength. Green arrows indicate the location of the stellar features, Mgb (5175 Å) and Fe (5270 Å).

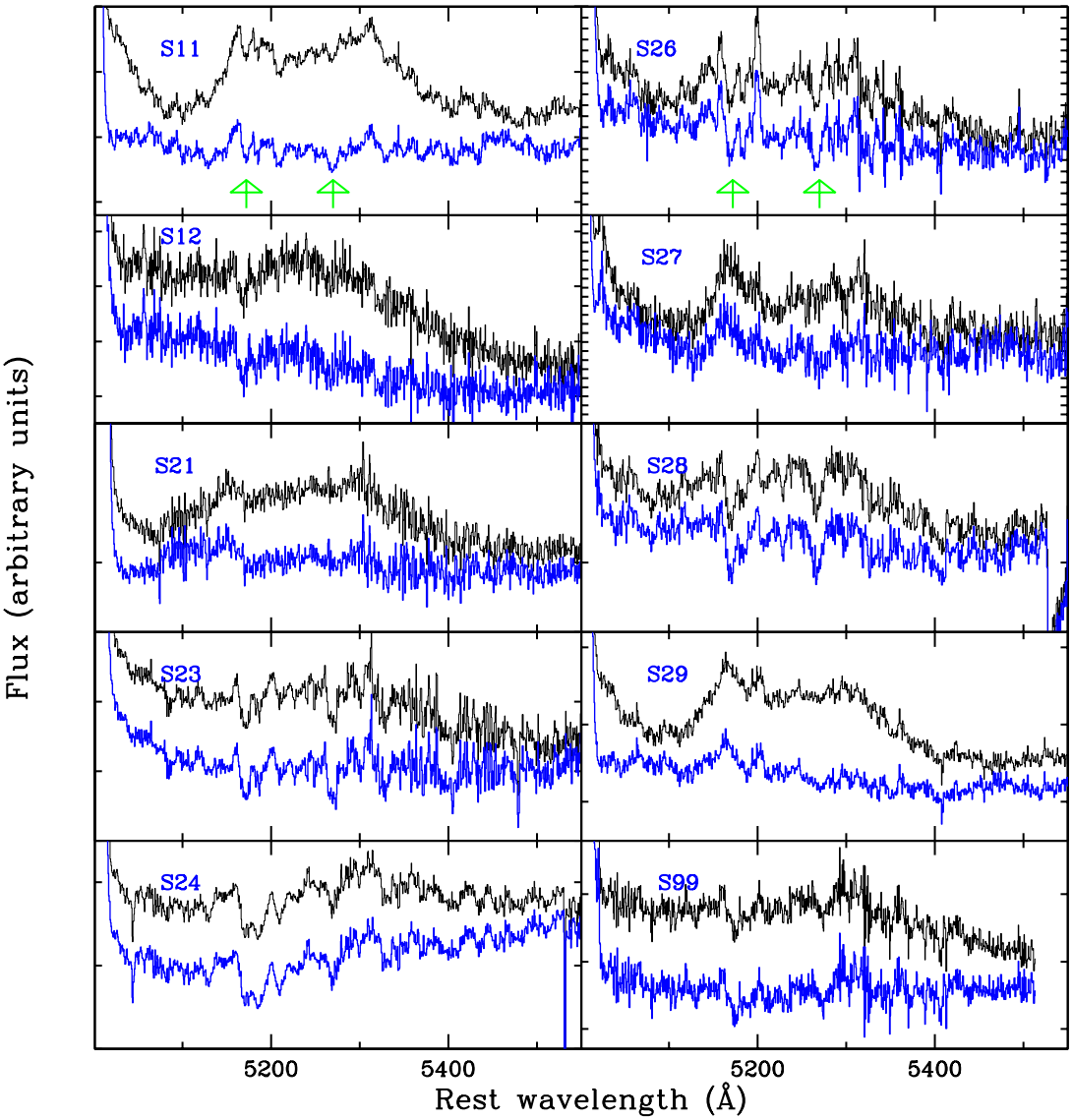

Fig. 3. — Continued.

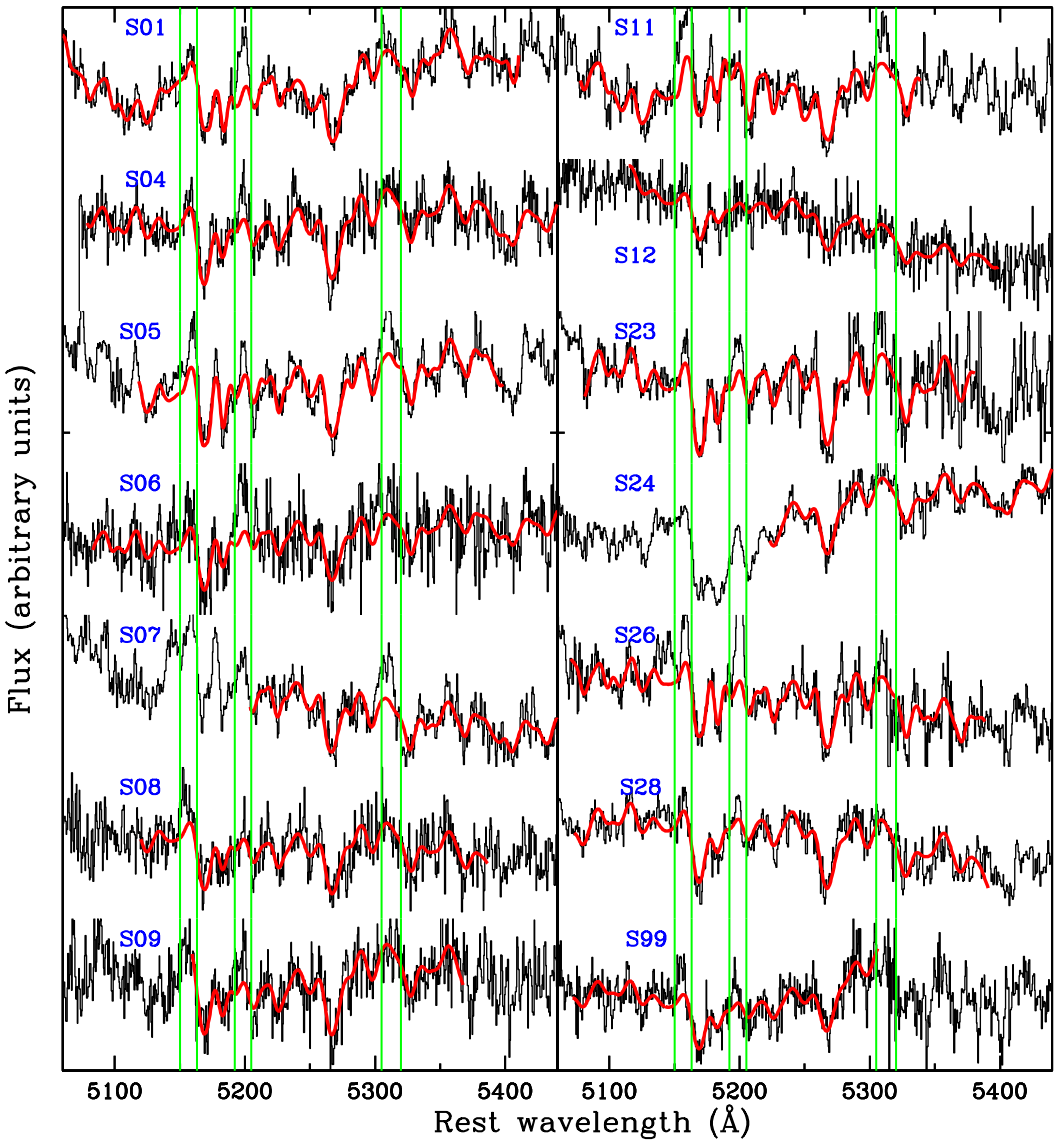

FIG. 4.— Velocity dispersion measurements. The region including the main stellar features around Mgb (5175)and Fe (5270) is shown (black histogram) together with the best fit template (red thick line). The regions around narrow AGN emission lines – identified by green vertical lines – are masked out before fitting.

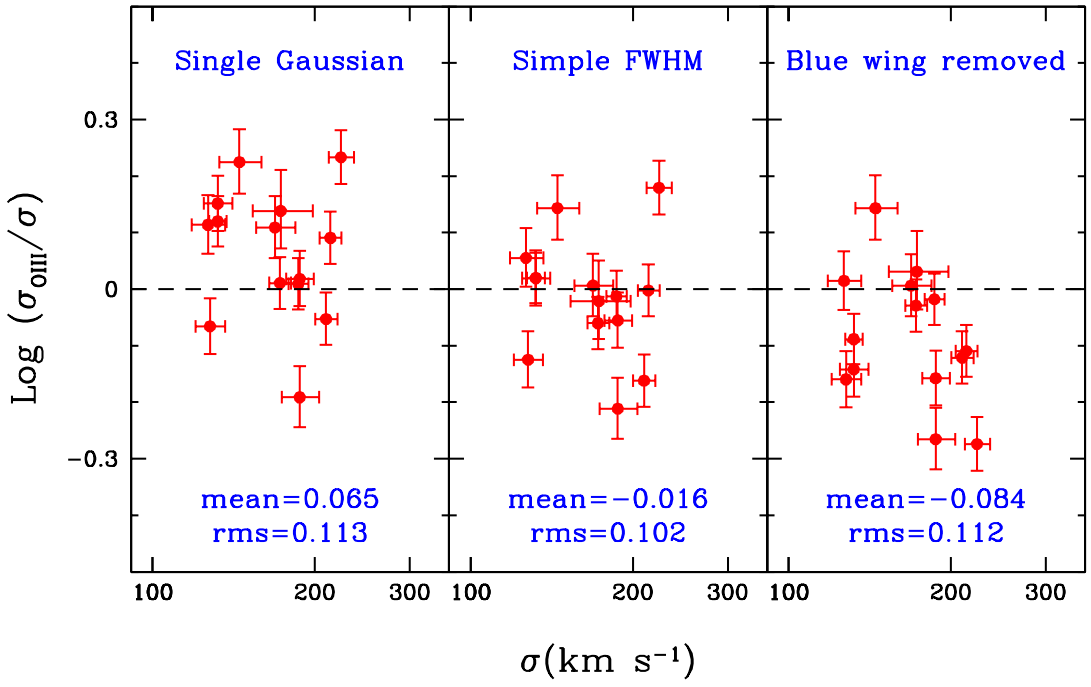

FIG. 5.— Comparison of velocity dispersion measured from stellar features and from the narrow [O III] line. From left to right, we compare with the stellar velocity dispersion a single gaussian fit to the emission line, the FWHM divided by 2.35, and a double gaussian fit. Note that the single gaussian fit provides a very bad fit to the data because the narrow lines are asymmetric with a prominent blue wing.

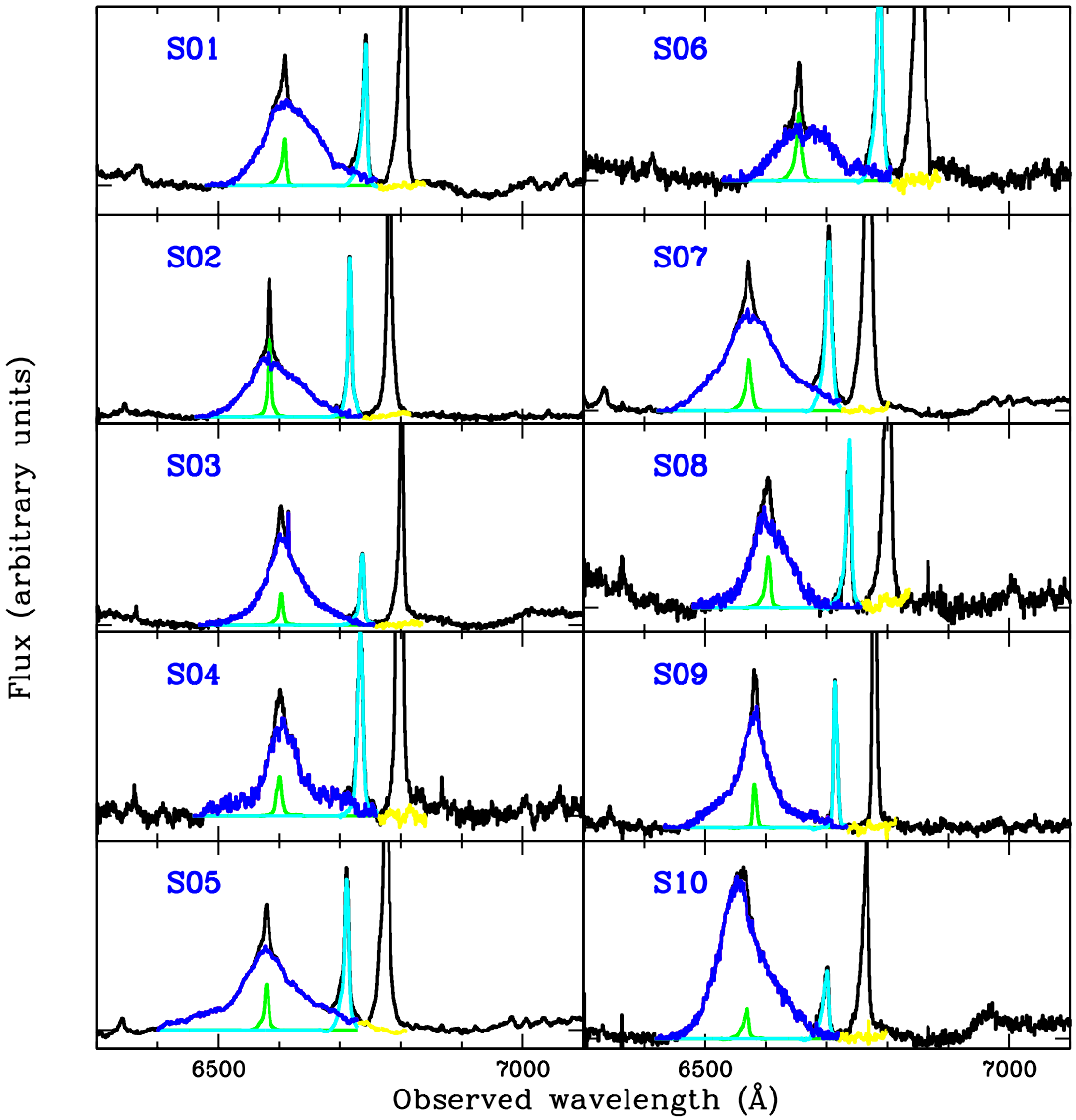

FIG. 6.— Determination of the second moment of broad Hβ. After removing the continuum (cyan horizontal line), [O III]λ5007 is rescaled and blueshifted to subtract [O III]λ4959 (cyan line) and the narrow core of Hβ (green line). The second moment is measured on the residual broad Hβ (blue histogram). See Section 4.1 for details.

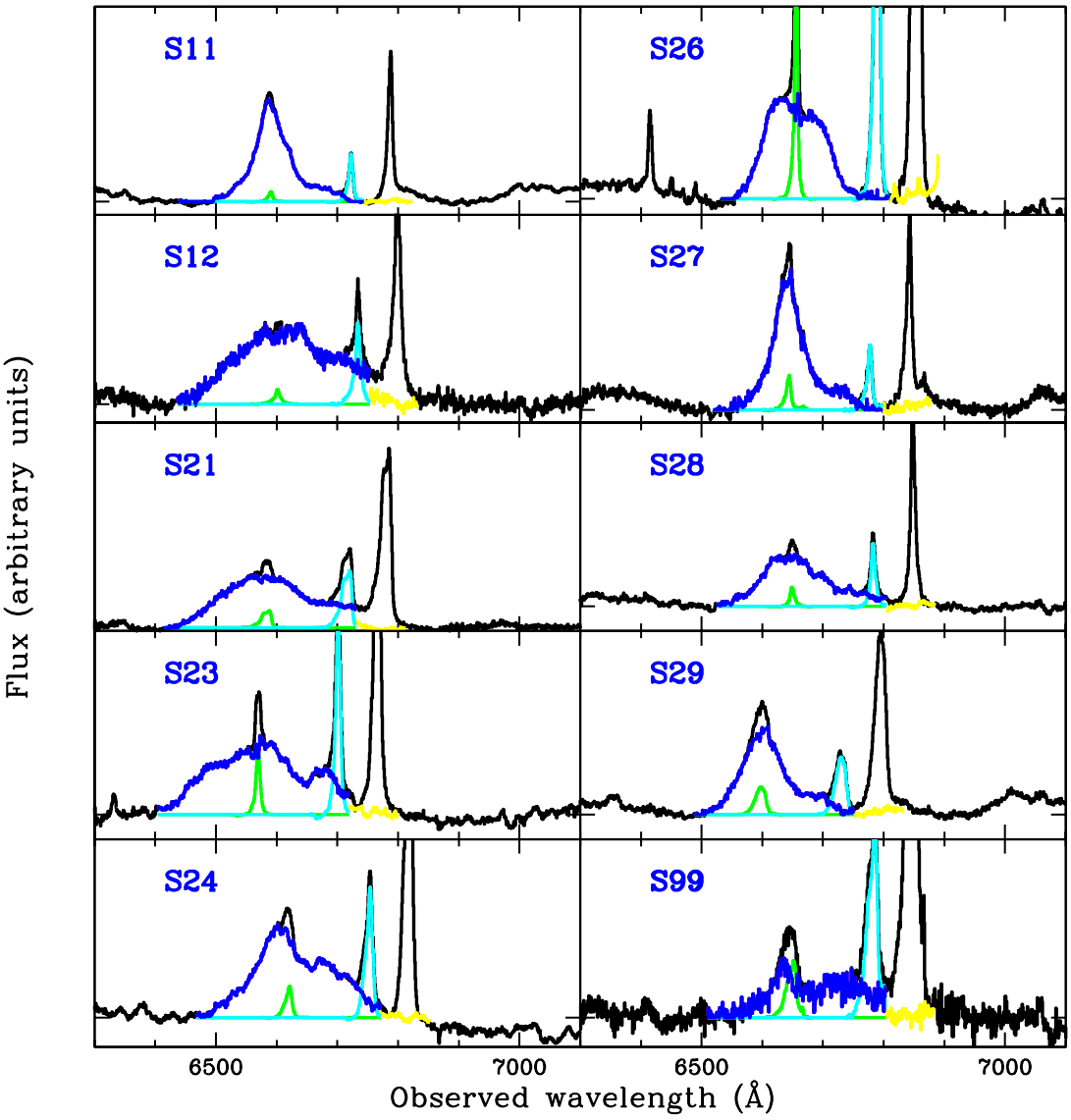

Fig. 6. — Continued.

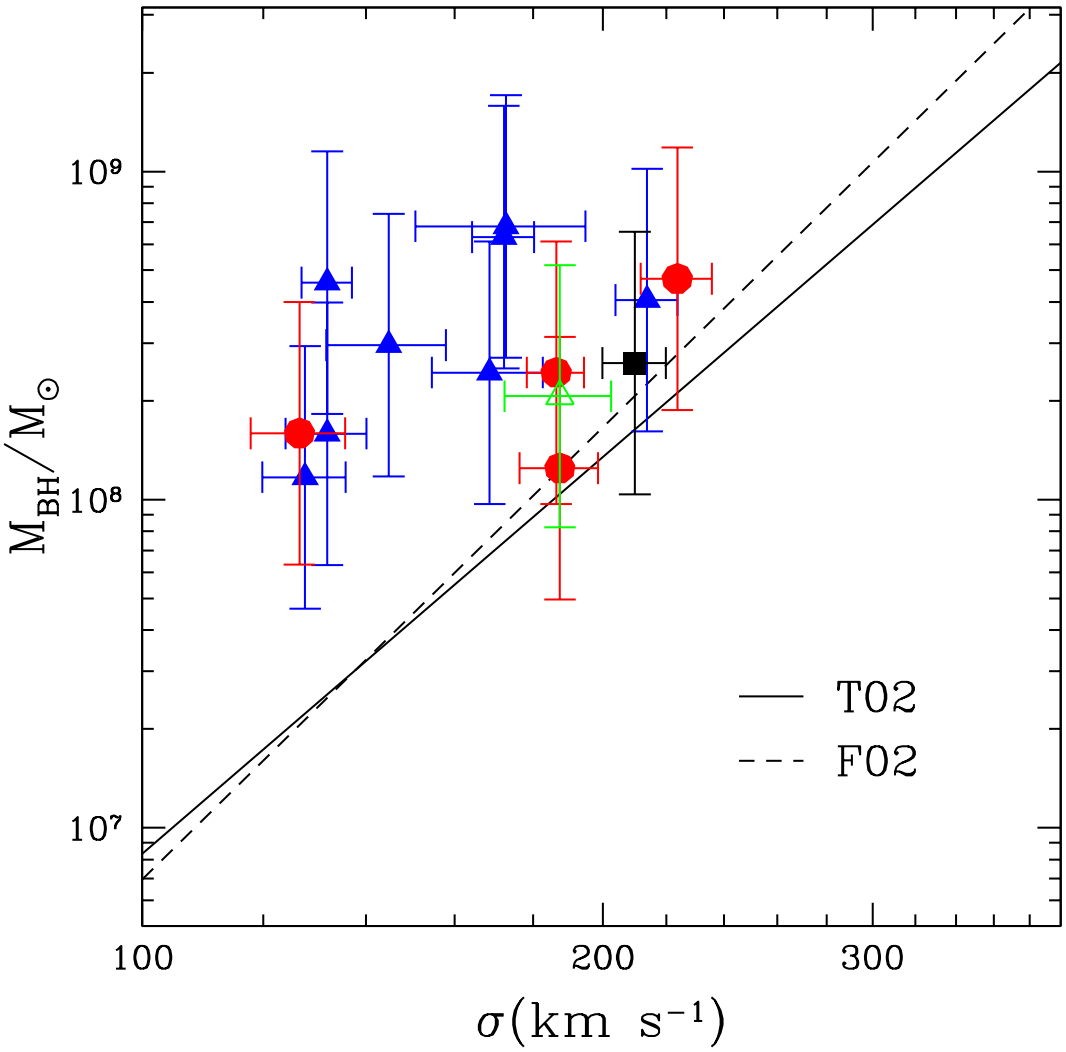

FIG. 7.— The $M_{BH} - \sigma$ relation for our sample of Seyfert galaxies at $z = 0.36$. The local relationships for quiescent galaxies as measured by Tremaine et al. (2002; T02; solid line) and by Ferrarese (2002; F02; dashed line) are shown for comparison. Note that the points at $z = 0.36$ lie above the local relationship, consistent with smaller velocity dispersions for given BH mass. Host galaxy morphological types from HST imaging are also shown: red circles identify early-type galaxies (E, S0, and Sa); blue solid triangles late-type galaxies; a green open triangle highly disturbed merging systems; a black solid square indicates no HST image available.

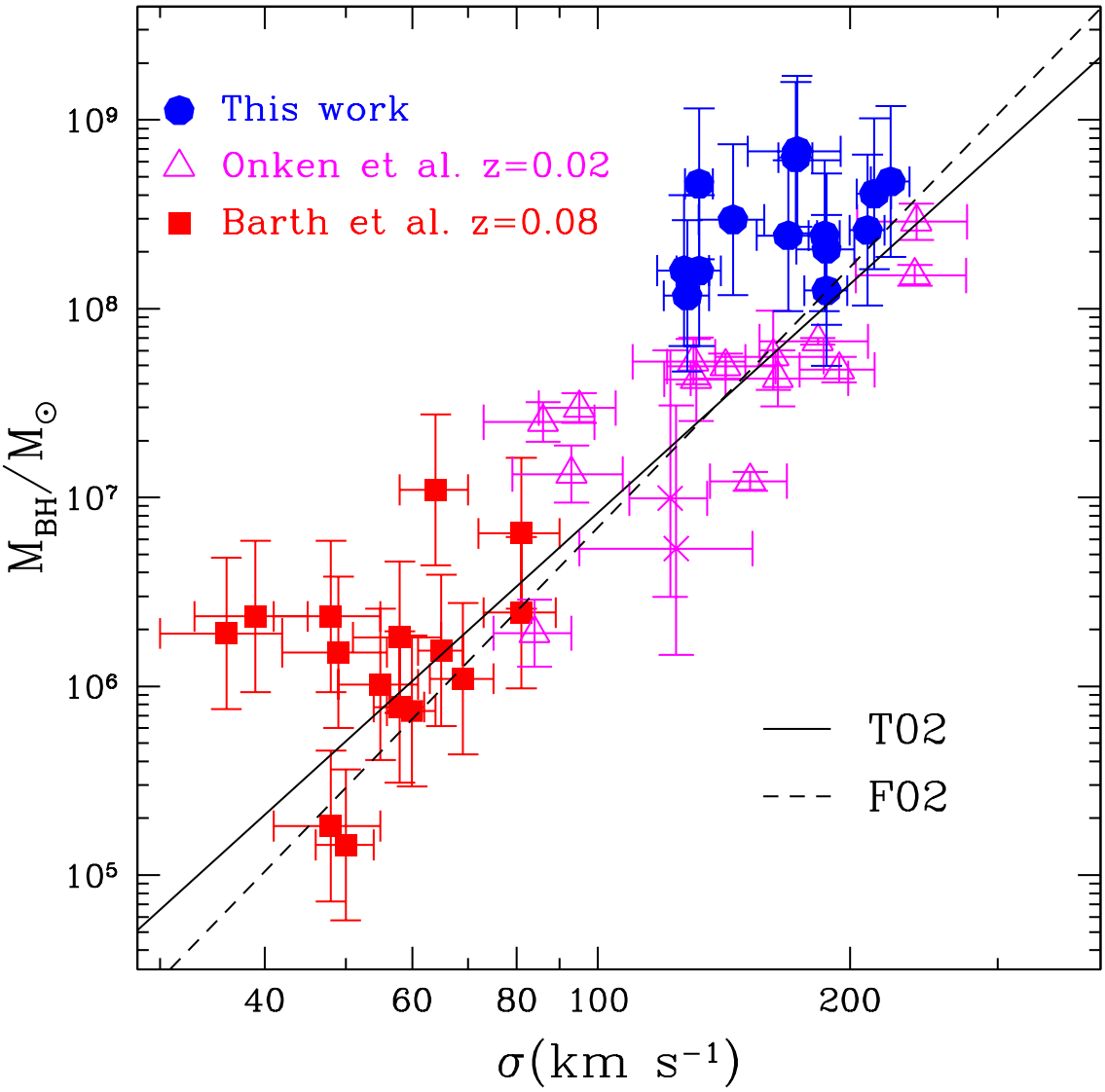

FIG. 8.— The $M_{BH} - \sigma$ relation of active galaxies. The symbols represent 14 Seyferts at $z = 0.36$ from this work (blue circles), 15 dwarf Seyfert galaxies at $z \sim 0.08$ from Barth et al. (2005; red squares), 14 local AGNs with BH masses measured via reverberation mapping from Onken et al. (2004; magenta triangles; two additional objects, excluded by Onken et al. and for consistency in our work, are shown as crosses). The local relationships of quiescent galaxies are shown for comparison as a solid (Tremaine et al. 2002) and dashed (Ferrarese 2002) line. Note that BH masses from this work and the Barth et al. sample adopt the same calibration of the shape factor as calculated by Onken et al. and therefore the relative position of the three samples along the y-axis is independent of the shape factor, provided it is redshift independent. Also, the shape factor given by Onken et al. 2004 is derived by requiring the local relationship for active and quiescent galaxies to be the same (see Onken et al. 2004 for details).

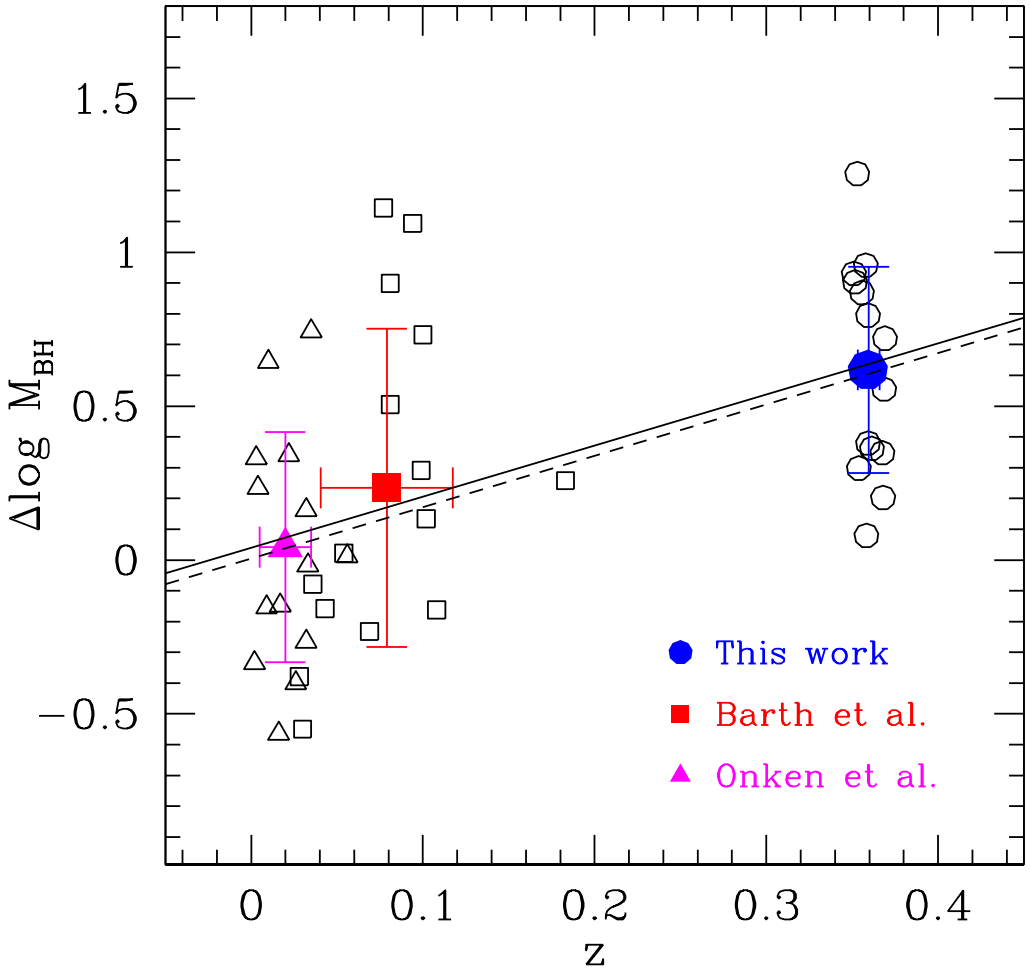

FIG. 9.— Offset from the local $M_{BH} - \sigma$ relation of Tremaine et al. (2002) for three sets of data (Onken et al. 2004 at $z \sim 0.02$; Barth et al 2005 at $z \sim 0.08$; our sample at $z = 0.36$). Large solid points with error bars represent the average and rms scatter for the three samples. The best linear fit to the data are shown as a solid line (for the three samples) and a dashed line (excluding the sample of dwarfs from Barth et al. 2005). The best fit linear relationship is $\Delta \log M_{BH} = (1.66 \pm 0.43)z + (0.04 \pm 0.09)$. The rms scatter of the $z = 0.36$ sample is 0.35 dex, similar to that of the Onken et al. points and to the estimated uncertainty on the BH mass determination via ECPI. The average offset of the $z = 0.36$ points is 0.62 ± 0.10 dex in BH mass corresponding to 0.15 dex in $\Delta \log \sigma$. Adopting the Ferrarese (2002) relationship leaves virtually unchanged the offset for our points (0.57 ± 0.11) and for the Onken et al. points, while increasing the offset of the Barth et al. (2005) sample significantly due to the large difference of the relationships for BH masses of order $10^6 M_\odot$ (see Figure 8). Including only our points and the Onken et al. points the offset with respect to the Ferrarese (2002) relation is $\Delta \log M_{BH} = (1.55 \pm 0.46)z + 0.01 \pm 0.12$.

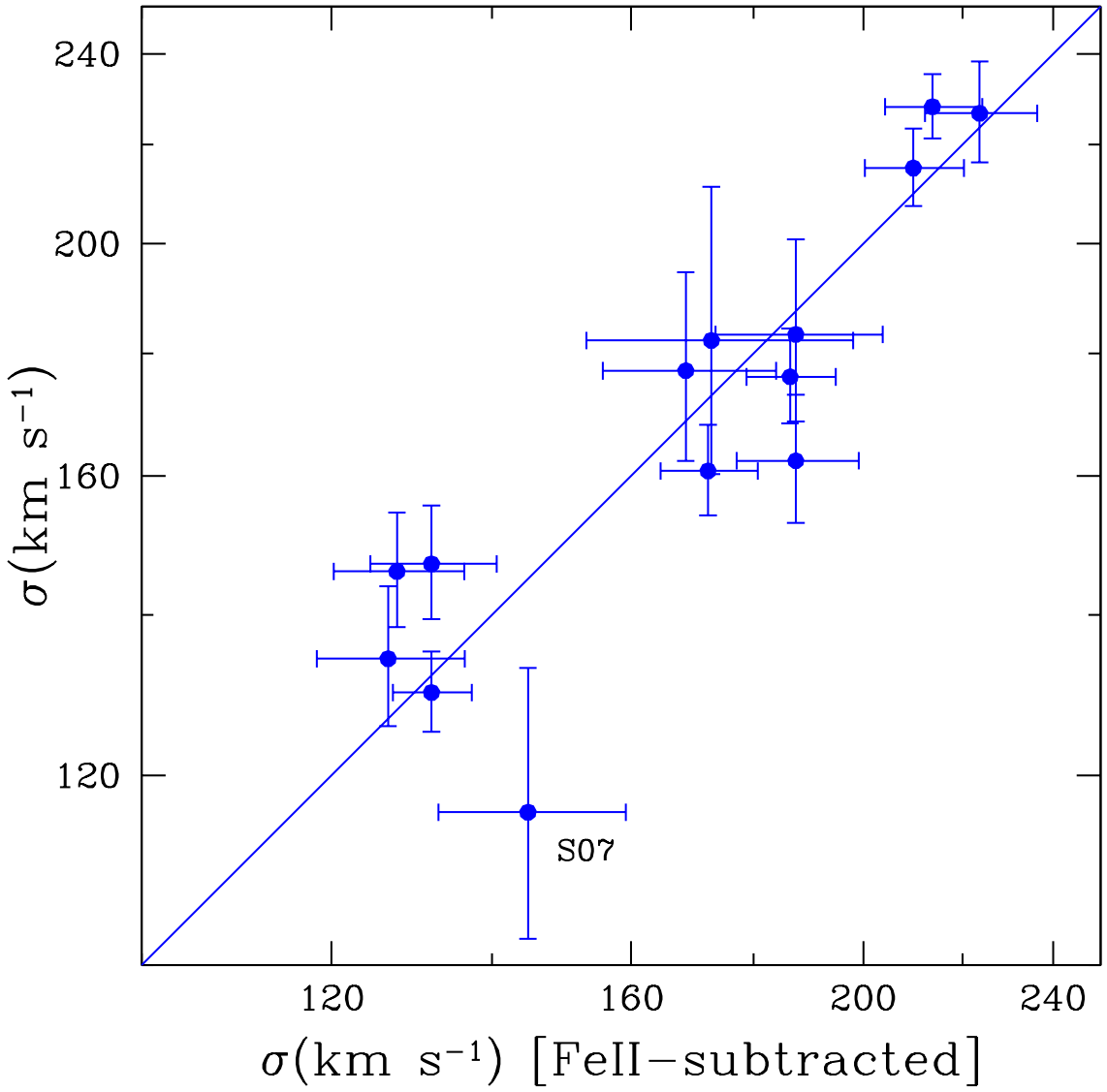

FIG. 10.— Comparison of stellar velocity dispersion measurements with and without the broad Fe II emission subtraction. The two measurements are consistent with mean offset of 0.01 dex and a rms scatter 0.04 dex. The most deviant point, S07, shows the strongest Fe II emission, consistent with showing the largest difference (∼0.1 dex).

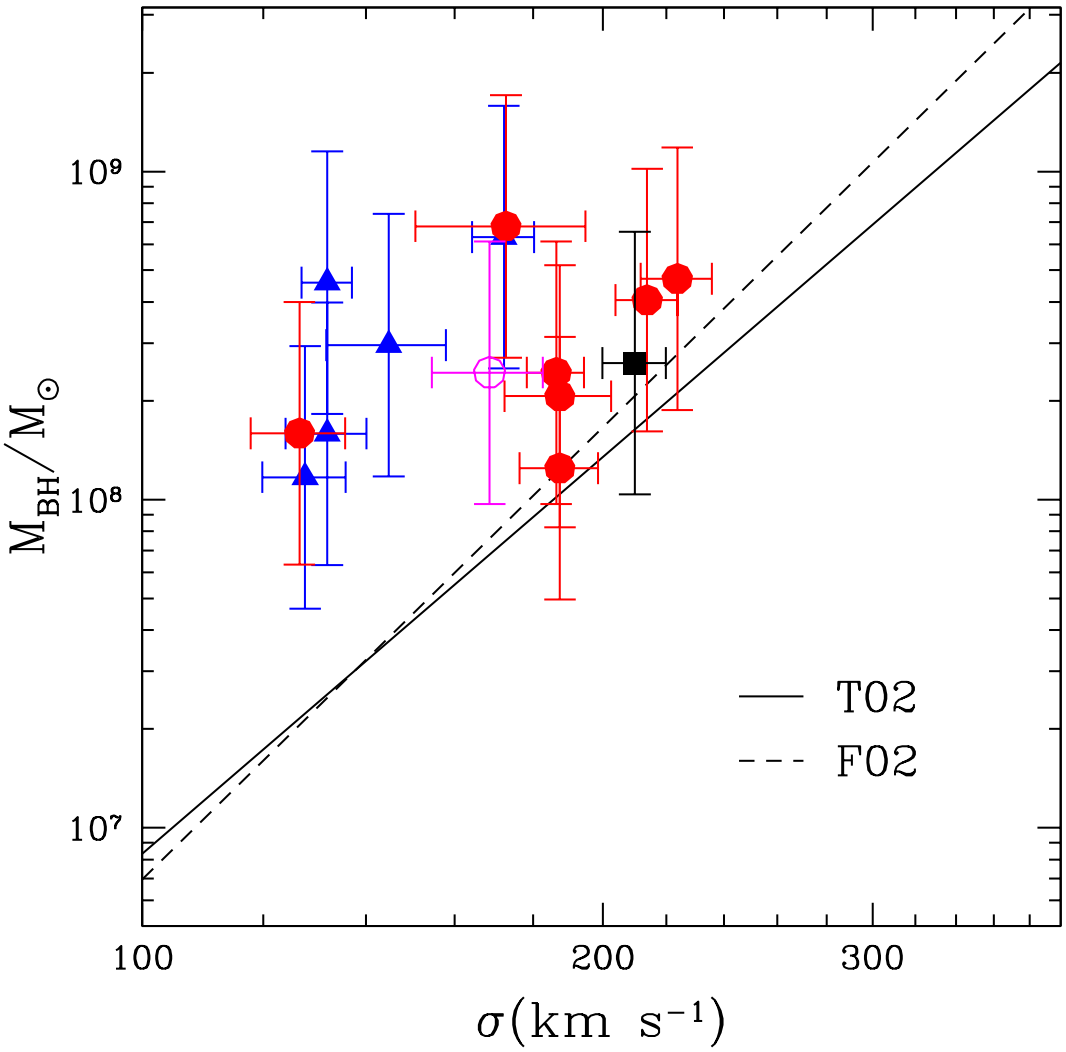

FIG. 11.— The $M_{BH} - \sigma$ relation depending on host galaxy inclination, as determined from HST images. Face-on galaxies (blue triangles) show smaller velocity dispersions compared to edge-on galaxies (open circle) and intermediate inclination + early-type galaxies (solid circles). A black square indicates an object without HST image. The offset without the face-on galaxies is 0.45 ± 0.10 in BH mass, 0.17 dex smaller than that of the total sample. The offset is found to be 0.92 ± 0.10 and 0.43 ± 0.10, respectively, for face-on galaxies and intermediate / undefined galaxies.

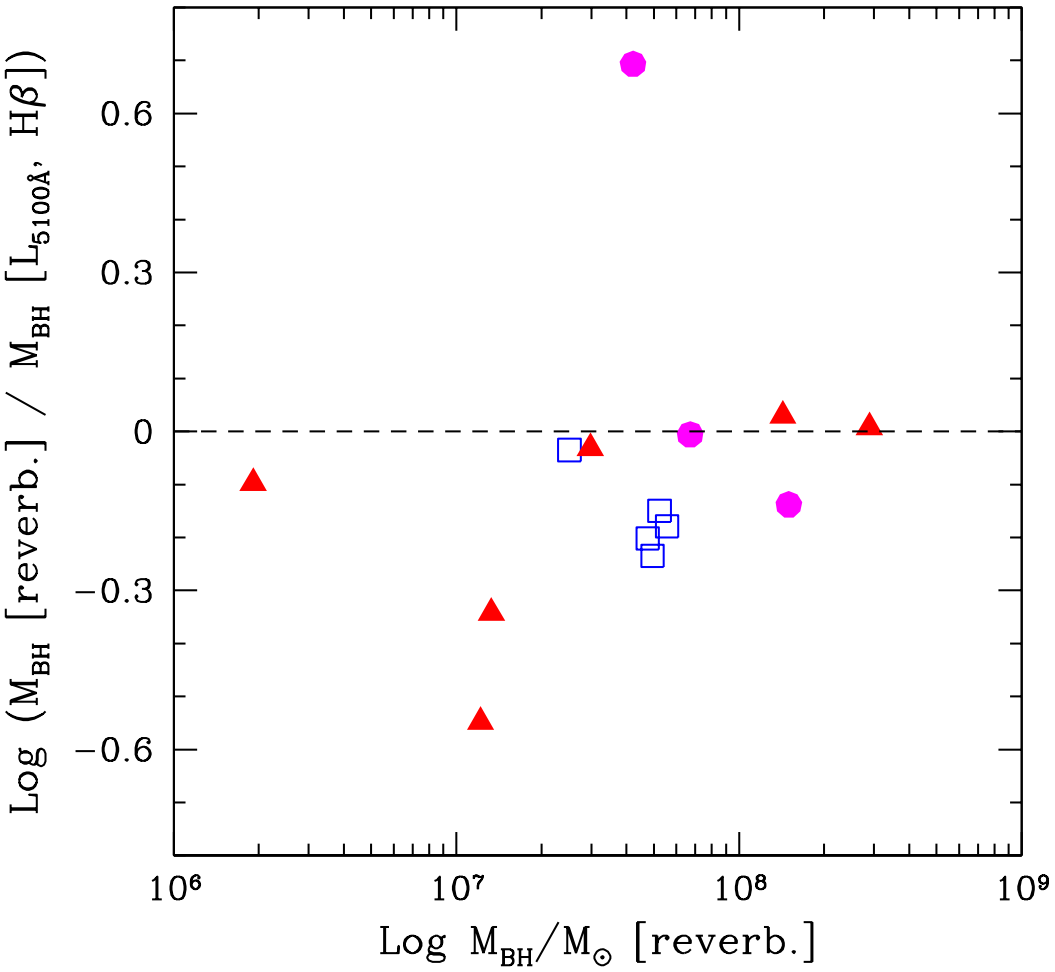

FIG. 12.— Comparison of BH mass obtained from reverberation results (from Peterson et al. 2004) and the ECPI method (i.e. from Hβ width and L_{5100} using Eq. 2) using single-epoch spectra (circles: spectra provided by A. Barth; triangles: spectra from International AGN Watch website) or mean spectra (squares: provided by B. Peterson). The mean offset is 0.09 ± 0.07 dex, indicating our Hβ width measurements from single-epoch data are consistent with those from the rms spectra.

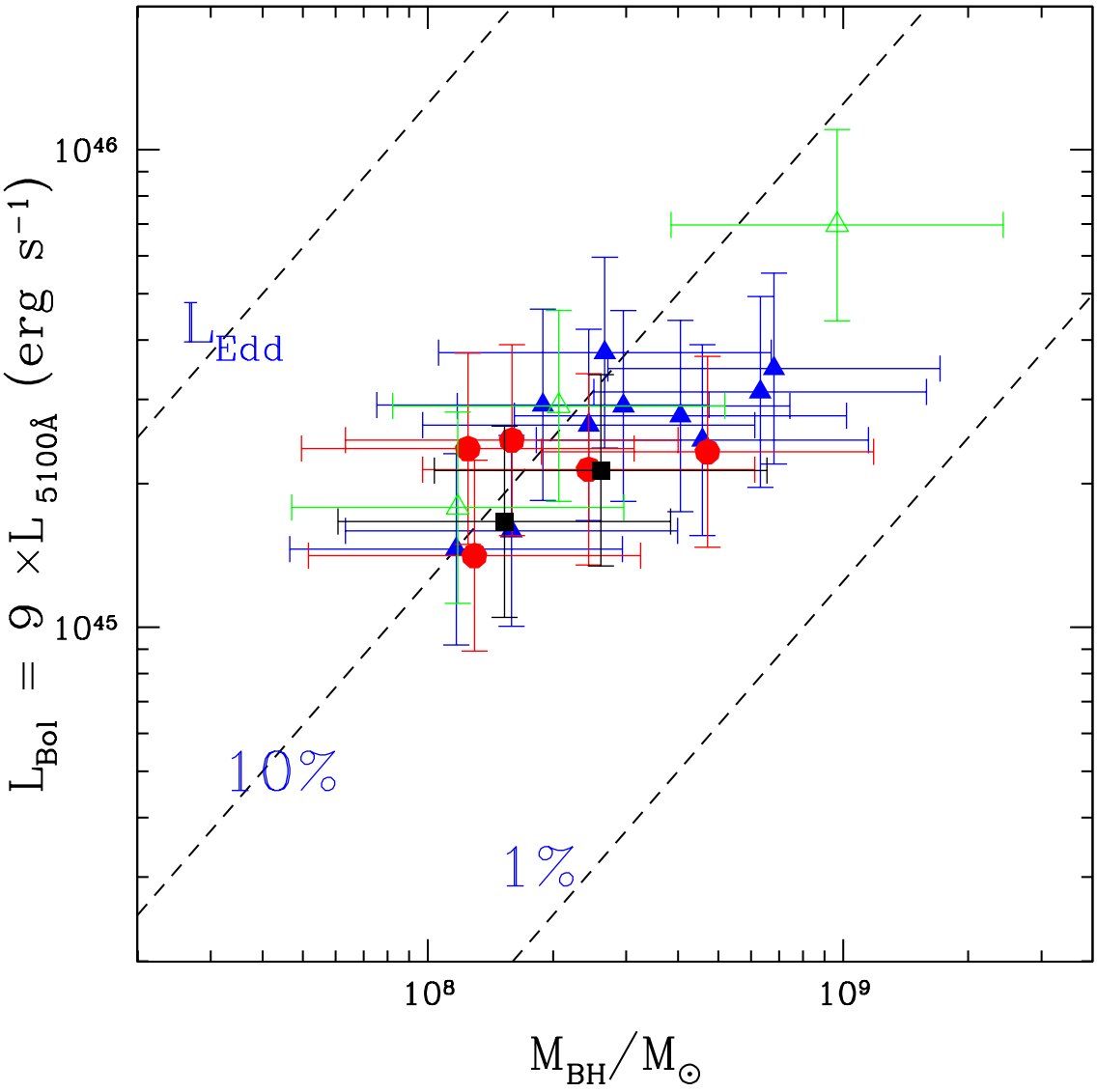

FIG. 13.— Bolometric luminosity vs. BH mass. Bolometric luminosities are calculated from optical luminosity multiplied by 9. Eddington ratios are indicated by dashed lines. Most of the observed Seyfert galaxies show low Eddington ratios, implying a low accretion rate. Symbols are same as in Fig. 7.